

CFD Analysis of Non-Newtonian Pseudo Plastic Liquid Flow through Bends

61(3), pp. 184-203, 2017

<https://doi.org/10.3311/PPme.9494>

Creative Commons Attribution 

Suman Debnath¹, Tarun Kanti Bandyopadhyay^{2*}, Apu Kumar Saha^{1**}

RESEARCH ARTICLE

Received 17 May 2016; accepted 03 October 2016

Abstract

Non-Newtonian pseudo plastic liquid flow through different types of 0.0127 m diameter pipe bends as well as straight pipe have been investigated experimentally to evaluate frictional pressure drop across the bends in laminar and water flow in turbulent condition. We have studied here the effect of flow rate, bend angle, fluid behavior on static pressure and pressure drop. A Computational Fluid Dynamics (CFD) based software is used to predict the static pressure, pressure drop, shear stress, shear strain, flow structure, friction factor, loss coefficient inside the bends for Sodium Carboxy Methyl Cellulose (SCMC) solution as a non-Newtonian pseudo plastic fluids and water as a Newtonian fluid. Laminar Non-Newtonian pseudo plastic Power law model is used for SCMC solution to numerically solve the continuity and the momentum equations. The experimental data are compared with the CFD generated data and is well matched. The software predicted data may be used to solve any industrial problem and also to design various equipment.

Keywords

fluent, CFD, bends, non-Newtonian pseudo plastic fluid, power law model, pressure drop, flow structure

1 Introduction

Non-Newtonian pseudo plastic fluid flow through bends are more complicated compared to the simple straight pipe as the bends are associated with different curve geometry. Bends are mainly used in petroleum and Refinery, Pharmaceutical, Rubber, Paper Pulp and Food industries as piping components for fluid transfer and as heat transfer equipment in boiler, heat exchanger, distillation column, and aircrafts. The idea of circulating blood flow pattern is different types of curved and bend blood vessels in aorta will help the doctors to identify the human diseases.

Since the bends are curved in nature, the fluids entering in the bend influence the combined centrifugal and viscous forces. We have considered Dean Number (De) to explain the flow phenomena inside the bends. The De plays a same role as Reynolds Number (Re) in a straight pipe. The velocity and pressure distribution inside the bends generate centrifugal and secondary flow which will transfer the denser fluid to the outer wall of the bend at a faster rate compared to the lighter fluid. The fluid will return to the inner wall side of the bend after collision with the outer wall. This creates a transverse pressure gradient in the form of kinetic energy and also pressure loss across the bend. The idea of fluid flow phenomena inside the pipe bends is important to design and analyze the fluid machinery. The prediction of pressure drop through bend is uncertain as the combined skin friction loss and loss due to changes in flow direction may explain the mechanism of flow phenomena inside the bends.

CFD analysis of non-Newtonian pseudo plastic flow through bends is important as it may be used as a complement to an experiment and also to lower the time and experimental cost of equipment. It gives us the conceptual studies of new design, redesign, detailed product development, troubleshooting with the help of numerical techniques where mass, momentum, energy, species are involved. The only disadvantage of this analysis is that the requirement of computer memory cost. The literature available for non-Newtonian pseudo plastic liquid flow through pipe bends are very less. So, the experimental and CFD analysis, both are required to predict the flow phenomena inside the bends.

¹ Department of Mathematics,
National Institute of Technology, Agartala

² Department of Chemical Engineering,
National Institute of Technology, Agartala

* First corresponding author, e-mail: tarunkantibanerjee0@gmail.com

** Second corresponding author, e-mail: apusaha_nita@yahoo.co.in

Dean [1, 2] first reported theoretically the laminar fully developed flow through a curved pipe. Berger et al. [3] explained the fluid flow phenomena inside the curved pipes and the laminar entrance flow through a curved pipe is explained by Soh and Berger [4]. Non-Newtonian liquid flow through bends is studied by S. K. Das, M. N. Biswas and A. K. Mitra [5]. Some studies of non-Newtonian fluid flow through curved pipes are reported by Mashelkar and Devrajan [6] and Mishra and Gupta [7]. Newtonian and non-Newtonian liquid flow through a variety of pipe fittings at low Reynolds numbers are reported by Edwards et al. [8]. Non-Newtonian pseudo plastic liquid flow through a small diameter piping components have been studied by Bandyopadhyay et al. [9]. Also, CFD analysis for non-Newtonian pseudo plastic liquid flow through elbows has been studied by Bandyopadhyay et al. [10]. The numerical simulation of gas-solid flow through U-bend is reported by Hidayat and Rasmuson [11]. The laminar flow of shear-thickening electrostatic ash-water mixture through a 90° pipe bend is numerically studied by Marn and Ternik [12]. Kuan et al. [13] showed numerical simulations for the flow of dilute gas-solid through a rectangular duct containing a horizontal to vertical bend angle of 90°. CFD analysis of erosion in the pipeline for slurry flow is investigated by Shah and Jain [14]. Wu and Chen [15] validated the experimental results with the CFD simulated data for Newtonian and non-Newtonian type of fluid in the pilot plant study for anaerobic digester. CFD analysis for Newtonian and non-Newtonian liquid flow through straight and helical coil was done by Manzar and Shah [16]. Athanasia Kalpakli [17] studied the turbulent flow through pipe bends. He also studied the Dean vortex secondary flow phenomena, flow structure and velocity profiles inside the bend. Numerical investigation of non-Newtonian microcirculatory blood flow in a hepatic lobule was done by H.P. Rani et al. [18]. Denis Doorly and Spencer Sherwin [19] studied the geometry and flow phenomena inside the curved pipes. Aidar Kadyirov [20] numerically investigated the swirl flow in a curved tube with various curvature ratio. CFD simulation of dilute gas-solid flow in 90° squares bend was studied by Tarek A. Mekhail [21]. P.L. Spedding [22] investigated the gas-liquid two-phase flow through 90° elbow-bends. Hidesato Ito [23] observed the secondary flow in the curved pipes. Gas particle flow through bends was studied by S Jayanti [24]. Modeling of flow phenomena inside the stenotic vessels was studied by S. A. Berger and L-D. Jou [25]. F. J. H. Gijssen et al. [26] studied the influence of non-Newtonian properties of blood flow in large arteries, unsteady flow in a 90° curved tube. M. Tanaka et al. [27] also studied the mechanics of Bio-fluids and computational analysis for peak systole. They observed the streamline flow phenomena at the peak systole.

Objective of the work

The frictional pressure drop, loss coefficient, shear stress, strain for non-Newtonian liquid flow through different types

of bend as piping components are evaluated by the CFD analysis. The secondary flow visualization inside the bends can be applied to the design of piping components to improve the flow characteristics. The CFD simulated data is validated with experimental data and it is helpful for the design of different types of bends used in fluid machinery and heat exchanging equipment. It is often helpful to optimize the pumping and design cost of the equipment. The information related to the obstruction of blood flow through the arteries can help the doctors to diagnose the diseases of sugar and cholesterol patients.

2 General equation of Bend

2.1 Dean number

A dimensionless number is given by Dean (1927, 1928) and is expressed as the ratio of the square root of the product of inertia and centrifugal forces to the viscous forces. This dimensionless number is called Dean Number (De).

De is introduced into the curved pipe to show the interaction between centrifugal and viscous forces. So, for curved pipe, De can be expressed as,

$$\frac{\Delta P}{\rho_l u^2} = F(De) \quad (1)$$

Where,

$$De = \text{Re} \left(\frac{r_{bp}}{r_{cb}} \right)^{\frac{1}{2}} = \text{Re} \left(\frac{d_{bp}}{d_{cb}} \right)^{\frac{1}{2}} \quad (2)$$

In this case, De plays a similar role as Re in a straight pipe.

2.2 Friction factor

The friction factor, f_{bp} for flow through a bend pipe is defined by the Fanning friction factor as,

$$f_{bp} = \frac{d_p \Delta P_{bp}}{2u^2 \rho_l L_{bp}} \quad (3)$$

The following modified equation is used for bend pipe:

$$f_{bp} = F(De_{bp}) \quad (4)$$

The following functional relationship is used to extend the applicability of the Eq. (3) with an angle factor to all the different bends in the horizontal plane:

$$f_{bp} = F\left(De_{bp}, \frac{\alpha}{180}\right) \quad (5)$$

When bend angle $\alpha \rightarrow 0$, radius of curvature of the bend, r_{cb} will be closed to zero, i.e. bend becomes straight and the friction factor, f_{bp} of Eq. (5) will be equal to the friction factor of the straight pipe, f_s . By incorporating the above limiting condition, Eq. (5) can be modified in the following manner:

$$\left(\frac{f_{bp}}{f_s} - 1 \right) = F\left(De_{bp}, \frac{\alpha}{180}\right) \quad (6)$$

3 The Experimental Setup

The schematic diagram of the experimental setup consists of 90° bend as shown in Fig. 1 (a). The different types of bends i.e. 30°, 60°, 90°, 120° and U have also been used and are shown in Fig. 1 (b) and their dimensions are given in Table 1. The experiment consists of a liquid storage tank (0.45 m³), test section, control and measuring systems for flow rates, pressure and other accessories. The test section consists of a horizontal upstream straight pipe of 1.2 m length, bend portion and a horizontal downstream straight pipe of 1.15m length. The reason for having long horizontal upstream and downstream pipes before and after the bend is to achieve a fully developed flow conditions to facilitate the measurement of pressure across the bend portion. The bend portion was connected to the upstream and downstream portions with the help of flanges. As per the experimental requirement, different types of bend angles are connected with the flanges and the position of the downstream and separator position were shifted. The piezometric ring was connected at different points of the upstream and downstream sections of the pipe as pressure taps. The difference between pressures across the bend is expressed as pressure drop. The bends used were of uniform internal diameter, constant curvature and roundness.

Table 1 Dimension of the different Bends

Type of Bend	Radius of curvature, r_{cb} (m)	Linear length of the Bends, L_{bp} (m)	Ratio of radius of tube to radius of curvature (r_{tp}/r_{cb})
30°	0.016	0.016	0.39687
60°	0.024	0.022	0.26458
90°	0.032	0.014	0.19843
120°	0.036	0.018	0.17638
U	0.052	0.028	0.12211

The experimental liquids were water, dilute solutions of SCMC (a high viscous grade, Loba Chemie Pvt. Ltd., Bombay, India) act as pseudo plastic fluids. The test liquids were prepared by dissolving the required amount of SCMC in tap water and kept stirring until a homogeneous solution was obtained after ageing for 10 h. Added trace amounts of formalin to prevent biological degradation. A cooling coil is incorporated in the liquid storage tank to control the liquid temperature. The liquid and air temperature used were closed to the atmospheric temperature, 31°C. Four aqueous solutions of SCMC with approximate concentrations of 0.2- 0.8 kg/m³ were used as the non-Newtonian liquid and the range of the variables are given in Table 2.

Table 2 Range of variables

Sl. No.	Parameters	Range of variables
1.	Bend angle (degree)	30°, 60°, 90°, 120° and U-bend
2.	Bend pipe diameter (m)	0.0127
3.	Liquid (SCMC solution) flow rate (m ³ /s)	$6 \times 10^{-5} - 45 \times 10^{-5}$
4.	SCMC (Sodium salt of Carboxy Methyl Cellulose) solution Conc. (kg/m ³)	0.2 – 0.8
5.	Density of the liquid SCMC solution (kg/m ³)	$1001.69 \leq \rho \leq 1003.83$
6.	Flow behavior index of the pseudoplastic liquid (SCMC solution)	$0.6015 \leq n' \leq 0.9013$
7.	Flow behavior index of SCMC solution ($Ns^{n'}/m^2$)	$0.0142 \leq K' \leq 0.7112$

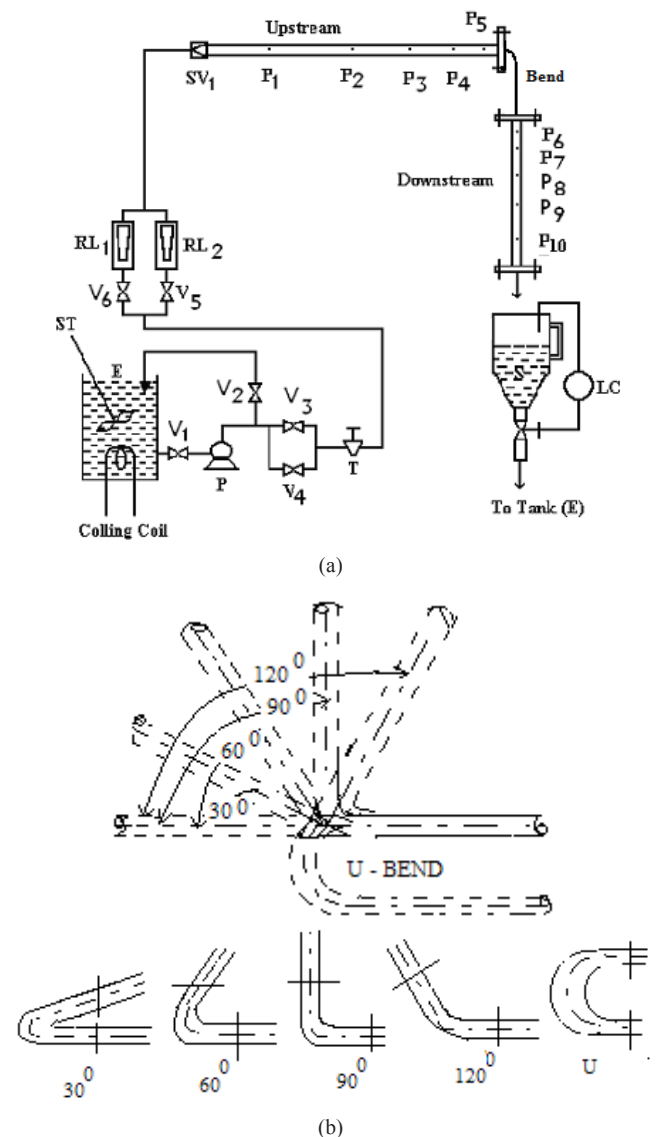


Fig. 1 (a) Schematic diagram of the experimental set up for bends E – tank; P – pump; S – separator; P₁ – P₁₀ – manometer toppings; LC – level controller; RL₁ – RL₂ – rota meters; ST – stirrer; SV₁ – solenoid valve; V₁ – V₆ – valves. (b) Types of bends.

4 CFD analysis

4.1 Mathematical Model

Dilute solutions of SCMC behave as a time independent non-Newtonian pseudo plastic fluids. The fluid follows the laminar non-Newtonian pseudo plastic power law model. The k-ε model is used for water in bends in a turbulent region. The apparent or effective viscosity, μ_{eff} are defined from Power law model for non-Newtonian fluids as,

$$\begin{aligned}\tau_{xy} &= K' \left| \frac{\partial u}{\partial y} \right|^{n'} = \frac{K' \left| \frac{\partial u}{\partial y} \right|^{n'} \left| \frac{\partial u}{\partial y} \right|}{\left| \frac{\partial u}{\partial y} \right|} = K' \left| \frac{\partial u}{\partial y} \right|^{n'-1} \left| \frac{\partial u}{\partial y} \right| \\ &= K' \left| \frac{\partial u}{\partial y} \right|^{n'-1} \left| \frac{\partial u}{\partial y} \right| = \mu_{eff} \left| \frac{\partial u}{\partial y} \right|\end{aligned}\quad (7)$$

Where,

$$\mu_{eff} = K' \left| \frac{\partial u}{\partial y} \right|^{n'-1} \quad (8)$$

Where, K' = consistency index and n' = flow behaviour index. The flow behaviour index, n' is an important parameter to subdivide the fluids as Newtonian ($n' = 1$), pseudo plastic ($n' < 1$) and dilatants ($n' > 1$). The deviation of n' from unity indicates the degree of deviation from Newtonian behaviour and ($n' < 1$) indicates the shear thinning behaviour of pseudo plastic fluids.

4.2 Measurement of rheological properties

Rheological properties and density of the solutions were measured experimentally by pipeline Viscometer and by the specific gravity bottle. The rheological properties, consistency and flow behavior index are obtained from the intercept and slope of the log-log plot of wall shear stress ($d_{bp} \Delta P / 4L$) vs. shear rate ($8u_1 / d_{bp}$). The basic relationship is developed by Metzner and Reed (1955) for power law fluid to relate pressure drop with the flow rate of SCMC solution by means of geometric parameters and the two physical properties of the fluid K' and n' as,

$$\frac{d_{bp} \Delta P}{4L} = K' \left(\frac{8u_1}{d_{bp}} \right)^{n'} \quad (9)$$

Where,

$$K' = \frac{K(3n'+1)}{4n'}$$

and

$$n' = \frac{d \left[\ln \left(\frac{d_{bp} \Delta P}{4L} \right) \right]}{d \left[\ln \left(\frac{8u}{d_{bp}} \right) \right]}$$

4.3 Governing equation

The effective viscosity is used for the calculation and defined as,

$$\mu_{eff} = K' \left(\frac{8u_1}{d_{bp}} \right)^{n'-1} \quad (10)$$

The governing continuity and momentum equations are the Navier-Stokes equation and can be written as,

Continuity equation:

$$\nabla u = 0 \quad (11)$$

Where, u is the non-Newtonian, SCMC solution velocity.

Momentum equation:

$$\rho \frac{\partial u}{\partial t} + \rho u \cdot \nabla u = \mu_{eff} \nabla^2 u - \nabla P \quad (12)$$

Where,

$$\nabla \equiv i \frac{\partial}{\partial x} + j \frac{\partial}{\partial y} + k \frac{\partial}{\partial z}$$

For steady non-Newtonian, SCMC solution flow, momentum equation is written as,

$$u \frac{\partial u}{\partial x} + v \frac{\partial u}{\partial y} = \left(\frac{1}{\rho} \right) \frac{\partial \tau_{xy}}{\partial y} \quad (13)$$

Where, u and v are the x and y velocity components respectively, τ_{xy} is the shear stress and ρ is the density of non-Newtonian pseudo plastic fluid (SCMC solution).

4.4 Boundary conditions

The continuity and momentum equations are solved subject to the following boundary conditions:

- Assuming bend walls are rigid and hence no slip conditions are introduced.
- Velocity is considered as inlet parameter and
- The outlet is the pressure of the fluid at the end of the pipe.

4.5 Assumptions of SCMC solution flow through bends

The following assumptions are taken for non-Newtonian pseudo plastic liquid flow through bends:

- The non-Newtonian pseudo plastic liquid flow through bends is 3-D fully developed and steady. For lowering the cost, we have used here fully developed i.e. the transition length of 50-80 ID for turbulent and laminar flow. The computer memory requirement was lowered during grid generation and simulation to minimize the convergence time.
- The fluid is isothermal, incompressible and non-Newtonian.
- The temperature of SCMC solution is fixed to 31°C.
- Single phase laminar pseudo plastic power law model is considered.

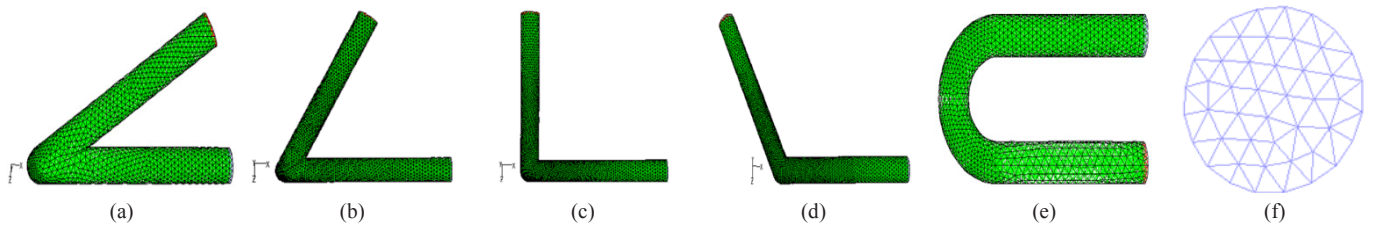


Fig. 2 Unstructured Tetrahedral grid; (a) 30° bend – Grid size: No. of cells = 17055; No. of faces = 36438; No. of nodes = 4105; (b) 60° bend – Grid size: No. of cells = 32481; No. of faces = 68734; No. of nodes = 7428; (c) 90° bend – Grid size: No. of cells = 39761; No. of faces = 84072; No. of nodes = 9044; (d) 120° bend – Grid size: No. of cells = 43688; No. of faces = 92374; No. of nodes = 9934; (e) U bend -Grid size: No. of cells = 19408; No. of faces = 40937; No. of nodes = 4396; (f) Tetrahedral grid for selected plane of the bend

(e) Non-Newtonian pseudo plastic and Newtonian water flow through bend is complex in nature. Secondary flow appears inside the bend. It is governed by the conservation of mass and momentum equation with laminar and turbulent flow condition.

4.6 CFD procedure

Mesh Geometries for the bends are created by using CFD preprocessor. The inlet is used to specify the inlet velocity and outlet is used to specify the pressure outlet. The mesh geometries of the bends are imported into CFD solver in 3-D, X, Y, Z Cartesian co-ordinate system. The pressure based CFD solver solved the governing equations in 3-D geometry. Laminar non-Newtonian Power Law model has been used for simulation. The model solves the Navier-stokes equation at prescribes velocities. The governing equations are nonlinear and several iterations of the loop must be performed before a convergent solution is obtained. The first-order upwind scheme is used in the discretization of a set of governing equations and interpolation schemes are used for calculating cell-face pressures using the segregated solver. Pressure-velocity coupling refers to the numerical algorithm which uses a combination of continuity and momentum equations to derive an equation for pressure (or pressure correction) while using the segregated solver. A Simple algorithm is used in CFD solver domains. The convergence criteria were set at 10^{-5} for momentum and 10^{-3} for continuity equation. The CFD based CGS solver is used for velocity and AMG solver is used for pressure correction.

5 Results and discussions

5.1 Numerical simulation

The CFD based software is used to numerically simulate the non-Newtonian pseudo plastic liquid flow through bends. Different geometries of bends are created depending on angle and mesh by using the CFD module. Unstructured grids with tetrahedral elements are used for generating meshes. A grid independence study was carried out by varying the number of elements in the bend domain. Grid having 17055-44000 elements with varying bend angles is found to be sufficient as any further refinement does not produce any change in velocity and pressure profiles

at various cross sections. Velocities corresponding to Reynolds number ranging from 200 to 3000 are used in the simulation for non-Newtonian pseudo plastic liquid flow through bends. The first order upwind scheme is used for calculation. A 3-D flow simulation over the entire length of the angular bends has been studied. The effect of various parameters: bend angle, pseudo plasticity, flow rate or velocity on viscosity, static pressure, pressure drop, shear stress, strain, friction factor, flow structure, Dean vortices, secondary flow phenomena have been explained clearly.

Fig. 2 (a) – (e) show the tetrahedral grid of 30°, 60°, 90°, 120° and U-bend. Fig. 2 (f) shows the tetrahedral grid for the selected plane of the bend.

5.2 Effect of bend angle on single-phase pressure drop

Fig. 3 (a) – (f) and Fig. 4 (a) – (f) show the effect of bend angle on static pressure. It is clear from the plot that as the bend angle increases, the single-phase pressure drop decreases at constant SCMC solution flow rate and concentration. The reason is that as the magnitude of the secondary flow and the centrifugal forces acting on the liquids are reduced with increasing bend angle and hence the single-phase pressure drop decreases. The increase of bend angle means low curve and large radius of curvature and hence more closer to behave as a straight pipe which can reduce the centrifugal and secondary forces on the fluid inside the bends and hence reduced the kinetic energy loss.

5.3 Effect of bend angle on velocity magnitude, velocity vector and dean vortices

Fig. 5 (a) – (e), Fig. 6 (a) – (f), Fig. 7 (a) – (f) and Fig. 8 (a) – (f) indicate the contour plot of velocity magnitude, velocity vector and dean vortices. From those plots, we observe that the intensities of velocity magnitude, velocity vector and dean vortices are diminished. This is due to the increase of bend angle, which lowers the intensities of secondary flow phenomena and hence reduce the centrifugal forces on the fluid inside the bend. The centrifugal force is, in principle, balanced by the pressure gradient in the plane of curvature. However, near the wall where the velocity is small, the pressure gradient can no

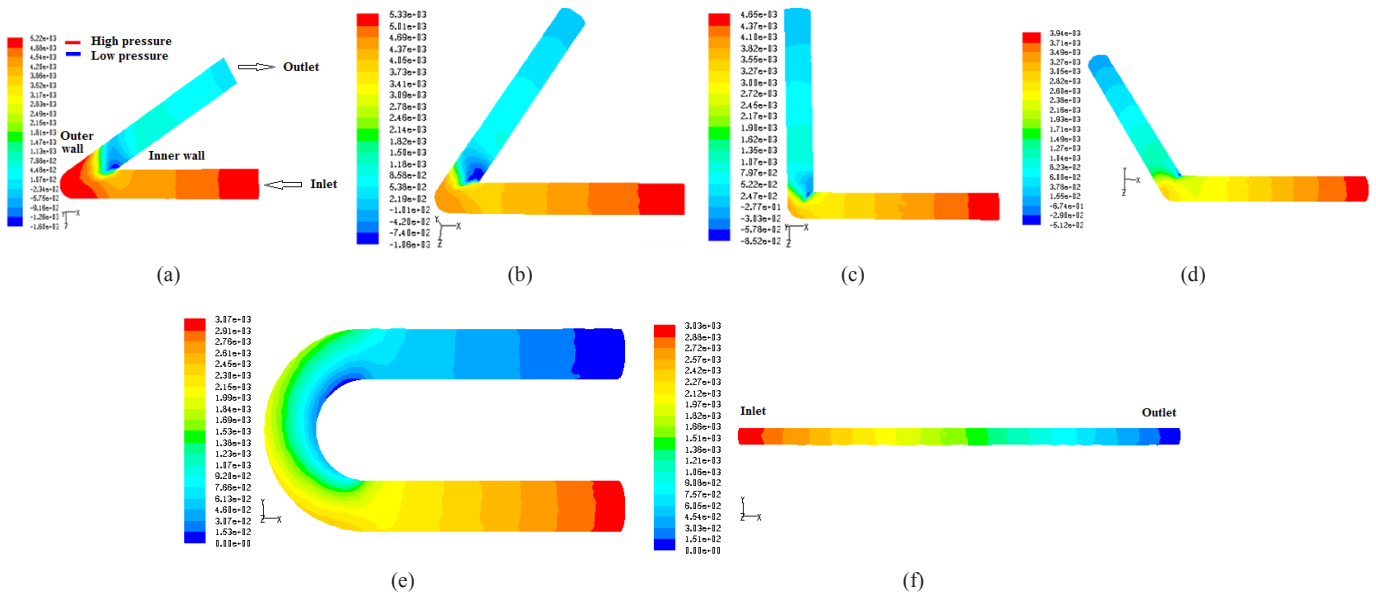


Fig. 3 Contour plot of static pressure (Pa) of the bends (a) 30° (b) 60° (c) 90° (d) 120° (e) U-bend (f) straight pipe, SMC solution Conc. (kg/m³): 0.8, Q₁(m³/s): 20 x 10⁻⁵

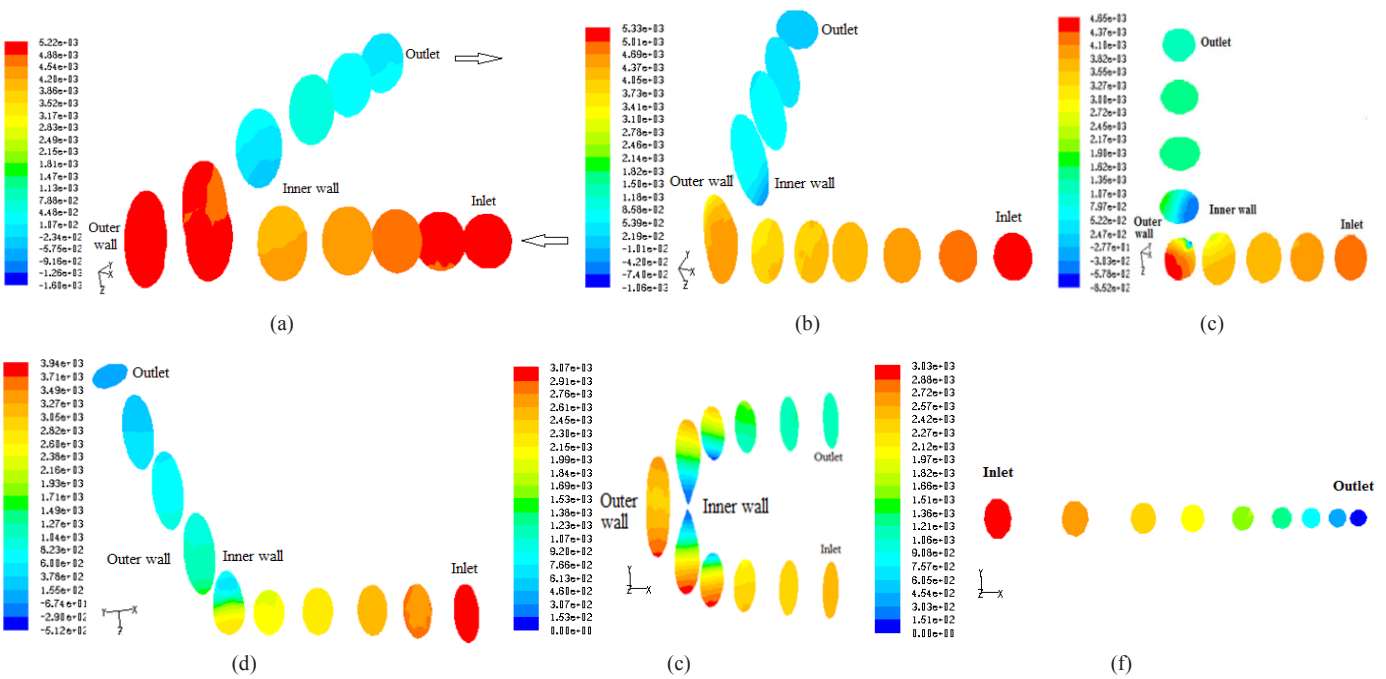


Fig. 4 Contour plot of static pressure (Pa) inside the different points of the bends (a) 30° (b) 60° (c) 90° (d) 120° (e) U-bend (f) straight pipe, SMC solution Conc. (kg/m³): 0.8, Q₁(m³/s): 20 x 10⁻⁵

longer be balanced and consequently fluid in the middle of the pipe moves to the outer wall and then turns to move inwards along the wall. The flow on the outer wall and separation at the inner wall make the flow very complex. The increase in bend angle, α lowers the magnitude of Dean Number of bend, $De_b = Re (r_{bp}/r_{cb})^{1/2} = Re (d_{bp}/d_{cb})^{1/2}$ and hence lower the curvature effect value of $(d_{bp}/d_{cb})^{1/2}$. In this case the curved bend behaves like a straight pipe where the radius of curvature will be $\alpha \rightarrow 0$ or $d_{cb} \rightarrow \infty$ and hence Re is important than De to lower the intensity of Dean Vortices.

5.4 Effect of bend angle on cell Reynolds number, dynamic pressure and vorticity magnitude

Fig. 9 (a) – (e), Fig. 10 (a) – (e), Fig. 11 (a) – (e) illustrate the contour plot of cell Reynolds number, dynamic pressure and vorticity magnitude. All are decreased with as increase in the bend angle. This is due to the decreasing of centrifugal forces.

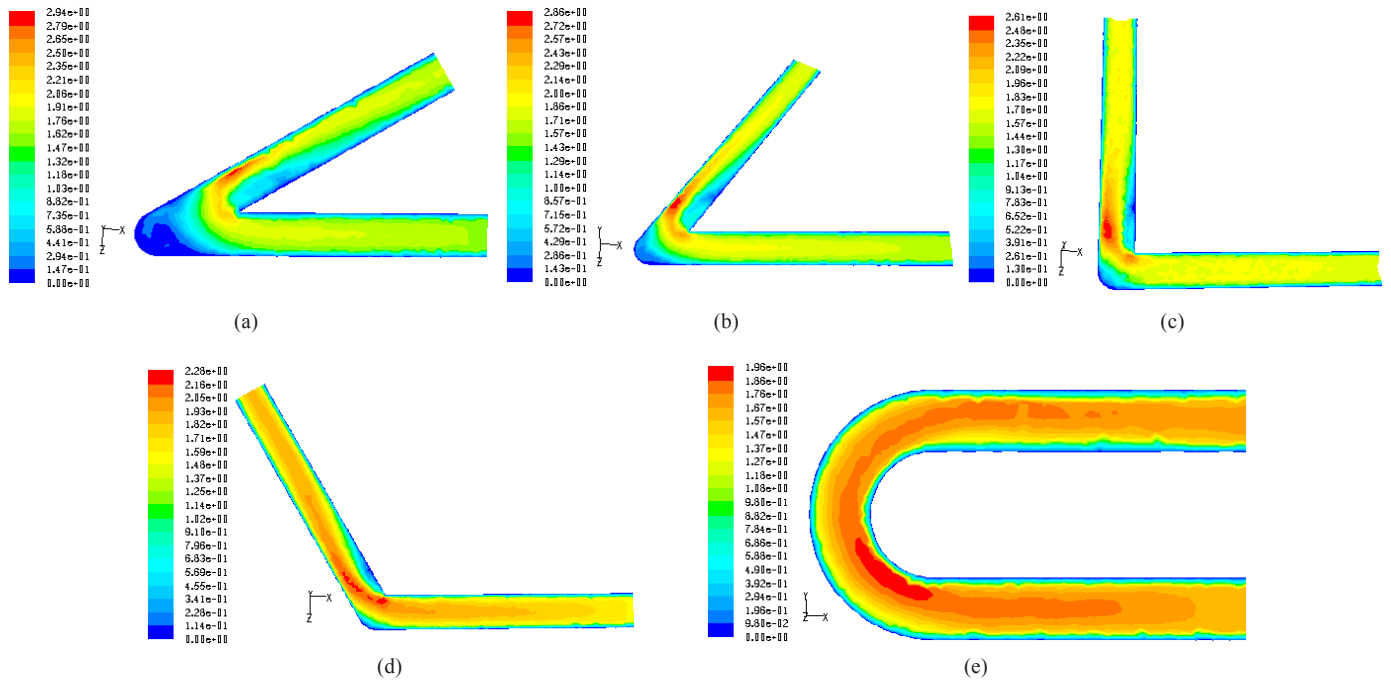


Fig. 5 Contour plot of velocity magnitude (m/s) of the bends (a) 30° (b) 60° (c) 90° (d) 120° (e) U-bend, SMC solution Conc. (kg/m³): 0.8, Q_i(m³/s): 20 x 10⁻⁵

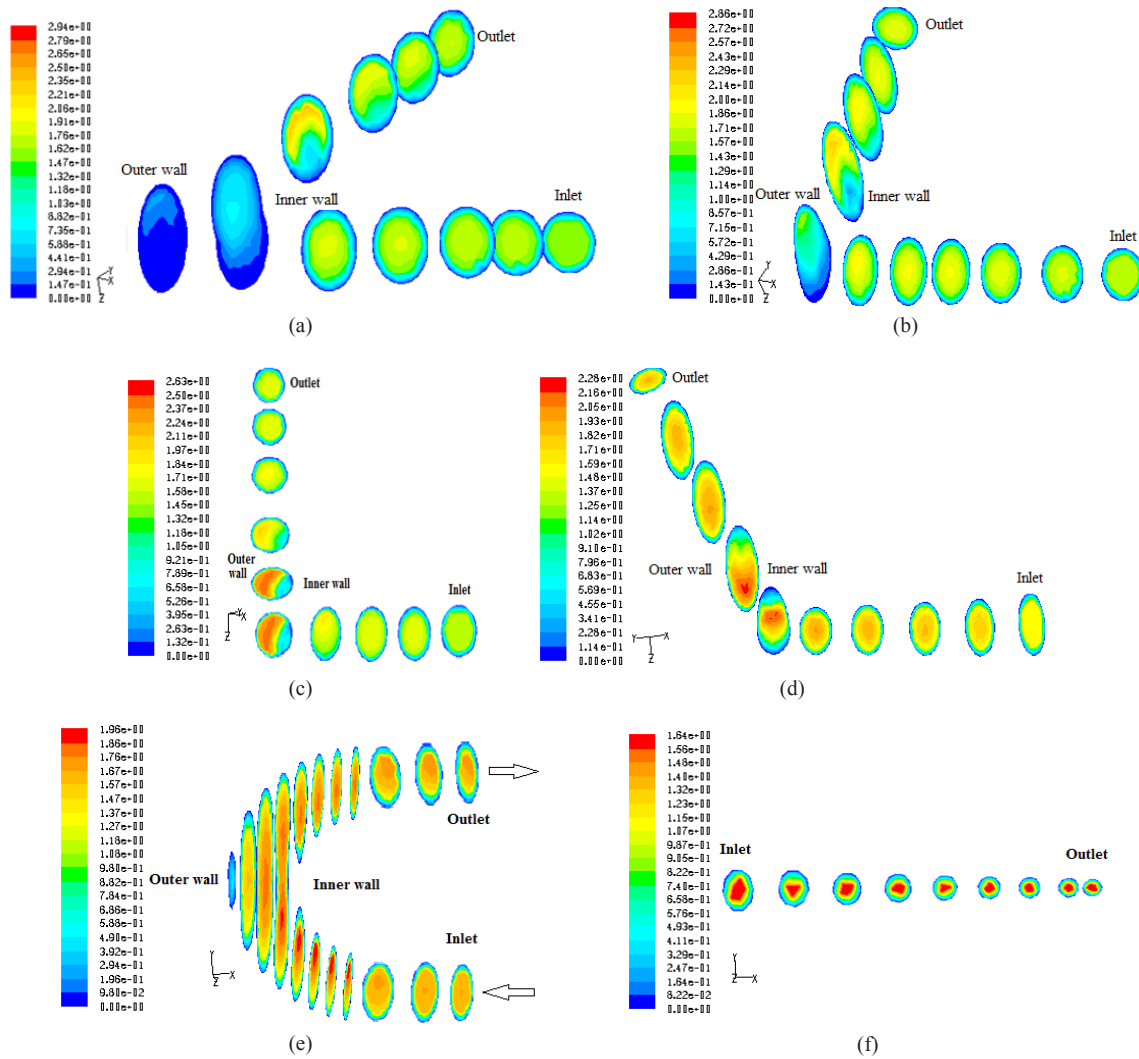


Fig. 6 Contour plot of velocity magnitude (m/s) inside the different points of the bends (a) 30° (b) 60° (c) 90° (d) 120° (e) U-bend (f) straight pipe, SMC solution Conc. (kg/m³): 0.8, Q_i(m³/s): 20 x 10⁻⁵

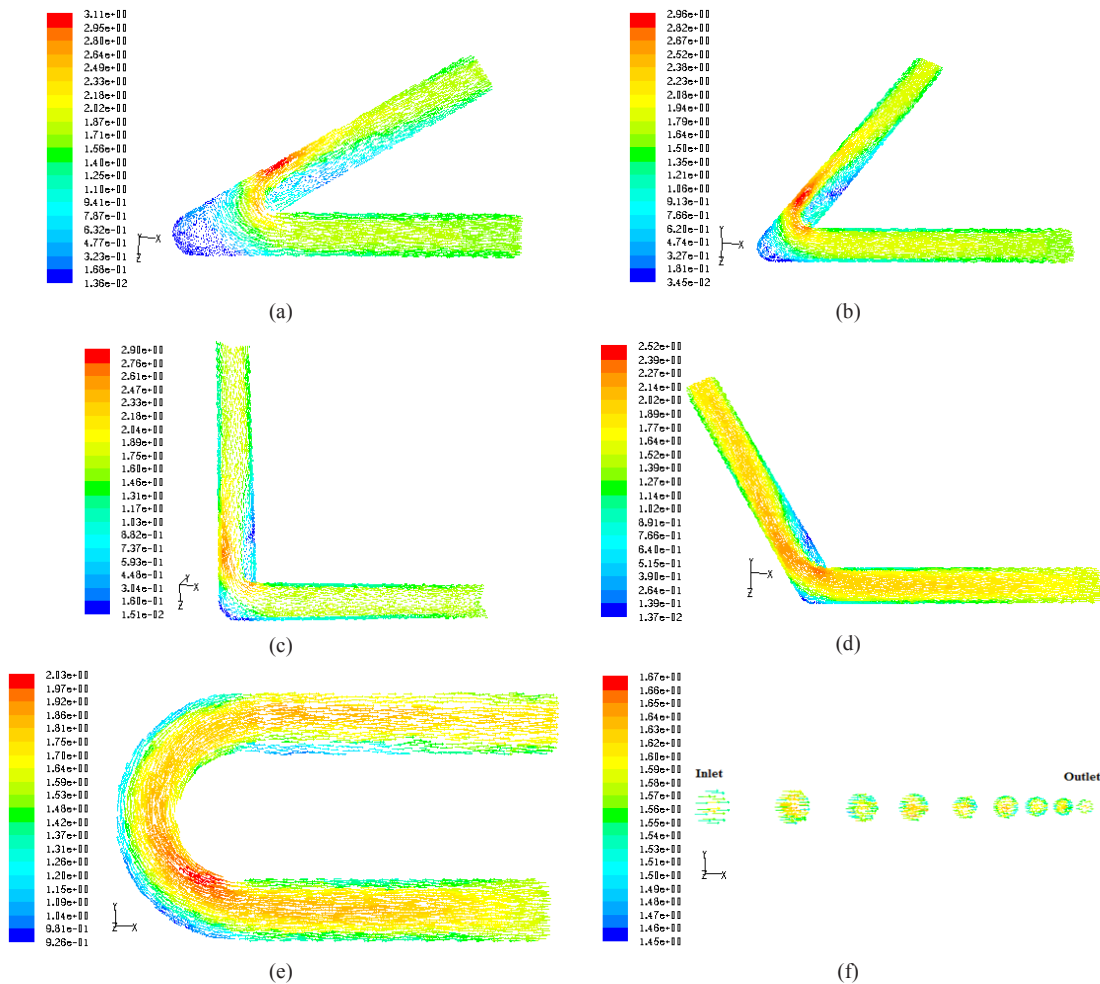


Fig. 7 Contour plot of velocity vector (m/s) of the bends (a) 30° (b) 60° (c) 90° (d) 120° (e) U-bend and (f) straight pipe, SMC solution Conc. (kg/m³): 0.8, Q₁(m³/s): 20 x 10⁻⁵

5.5 Effect of bend angle on wall shear stress and strain rates

Fig. 12 (a) – (f) and Fig. 13 (a) – (f) show the contour plot of wall shear stress and strain rates which are decreasing with increasing bend angle. The effects are less pronounced with increasing bend angle as the magnitude of $\tau_{\theta\theta}$ components are decreased with angle and thus the magnitude of low angular velocity (ω) lowers the values of shear stress and strain rate. The shear stress and strain are relatively more near the wall side compared to the central position of the pipe bend as the velocity variation between the fluid layers is more near the wall side compare to the central position.

5.6 Effect of liquid flow rate on single-phase drop, velocity, velocity vector

Fig. 14 (a) – (d) and (e) – (h), indicate the contours of static pressure at low and high Reynolds Number. It has been observed that the static pressure is high for SMC solution at high flow rates compared to water. This is due to the high angular momentum, centrifugal forces for more dense high viscous SMC fluid compare to the less dense water. Fig. 15 (a) – (d) and (e) – (h), Fig. 16 (a) – (d) and (e) – (h) illustrate the velocity

and velocity vectors for 90° and 120° bend for SMC solution and the water flow at high and low Reynolds number. The plots indicate that the fluid changes its flow direction when entering in the bend portion from the straight section of the pipe. Most of the time, the fluids are located at the centre portion of the straight pipe, but when fluids are entering into the bend portion, the fluids first reach to the outer wall portion of the bend. This is due to the high centrifugal forces generated from the heavier density SMC solution compared to the less dense water. The fluids then return to the centre and the inner wall side of the bend after collision with the outer wall of the bend. The secondary flow through bend is induced by the centrifugal forces and its interactions, primarily with viscous forces, is extremely important. The Dean number is defined as the ratio of the square root of the product of the inertial and centrifugal forces to the viscous force, incorporates all the forces for flow through bends. As a result, combination of both forces creates more intensity of centrifugal forces on the heavier density SMC solution fluids compared to the less dense water. The result will be more for low angle 90° bend compare to the large angular 120° bend and for higher Reynolds number, higher angular momentum compared to the low Reynolds Number, lower angular momentum.

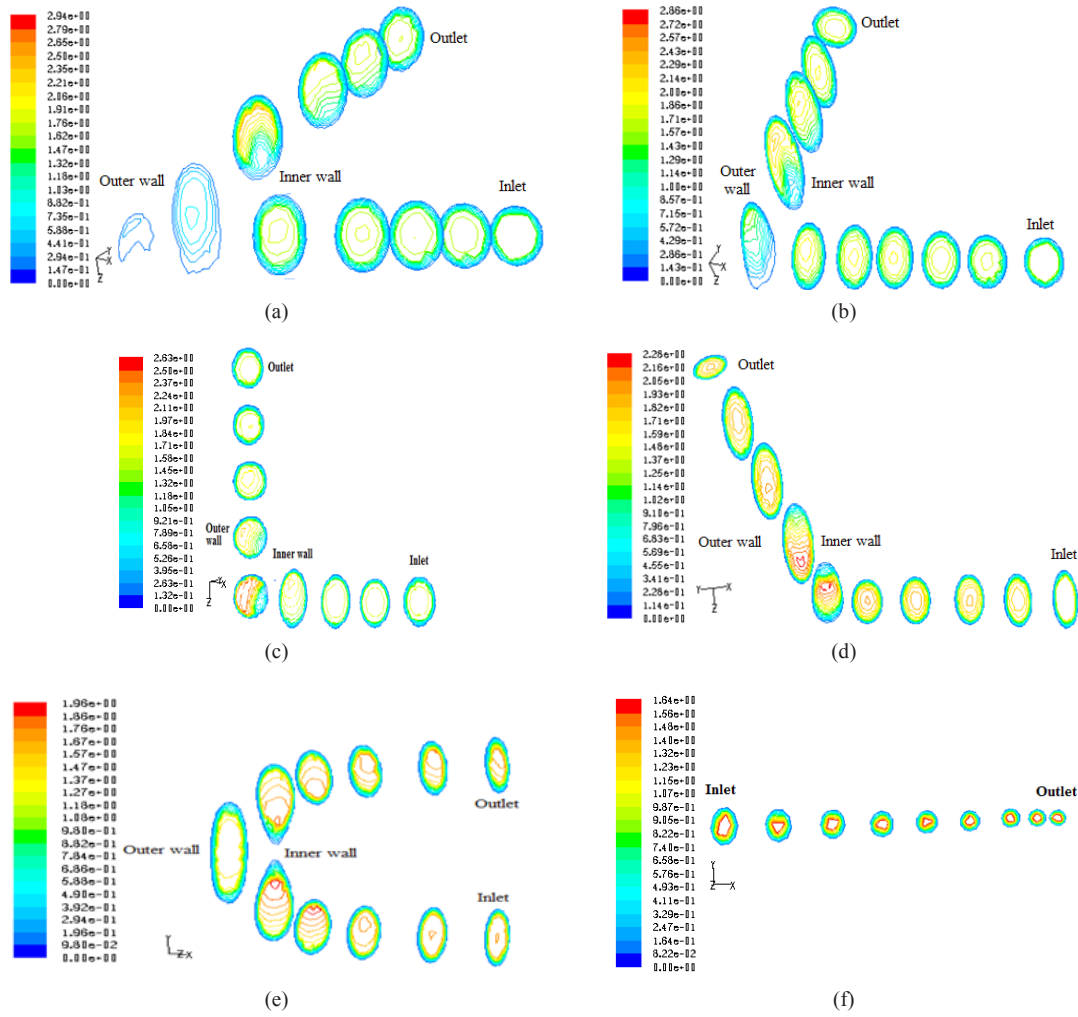


Fig. 8 Dean vortices inside the different points of the bends (a) 30° (b) 60° (c) 90° (d) 120°
 (e) U-bend (f) straight pipe, SMC solution Conc. (kg/m³): 0.8, Q_i(m³/s): 20 x 10⁻⁵

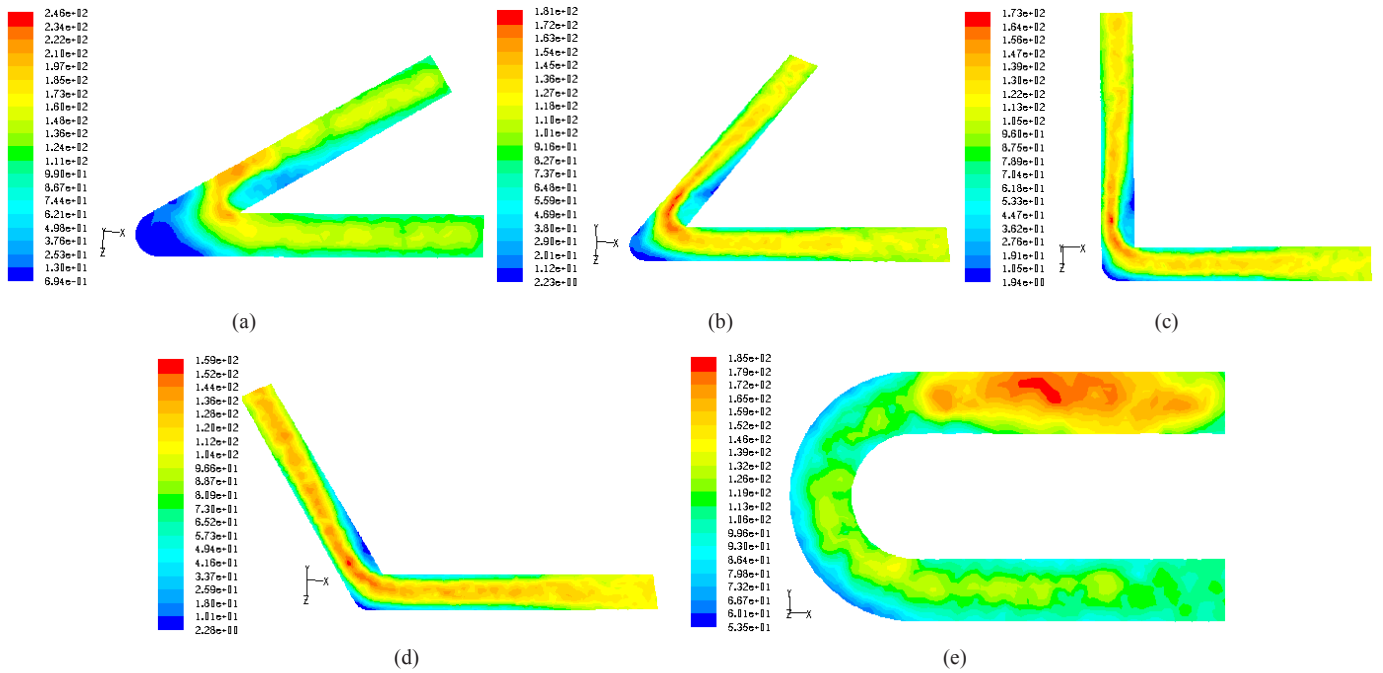


Fig. 9 Contours of Cell Reynolds Number of the bends (a) 30° (b) 60° (c) 90° (d) 120° (e) U-bend, SMC solution Conc. (kg/m³): 0.8, Q_i(m³/s): 20 x 10⁻⁵

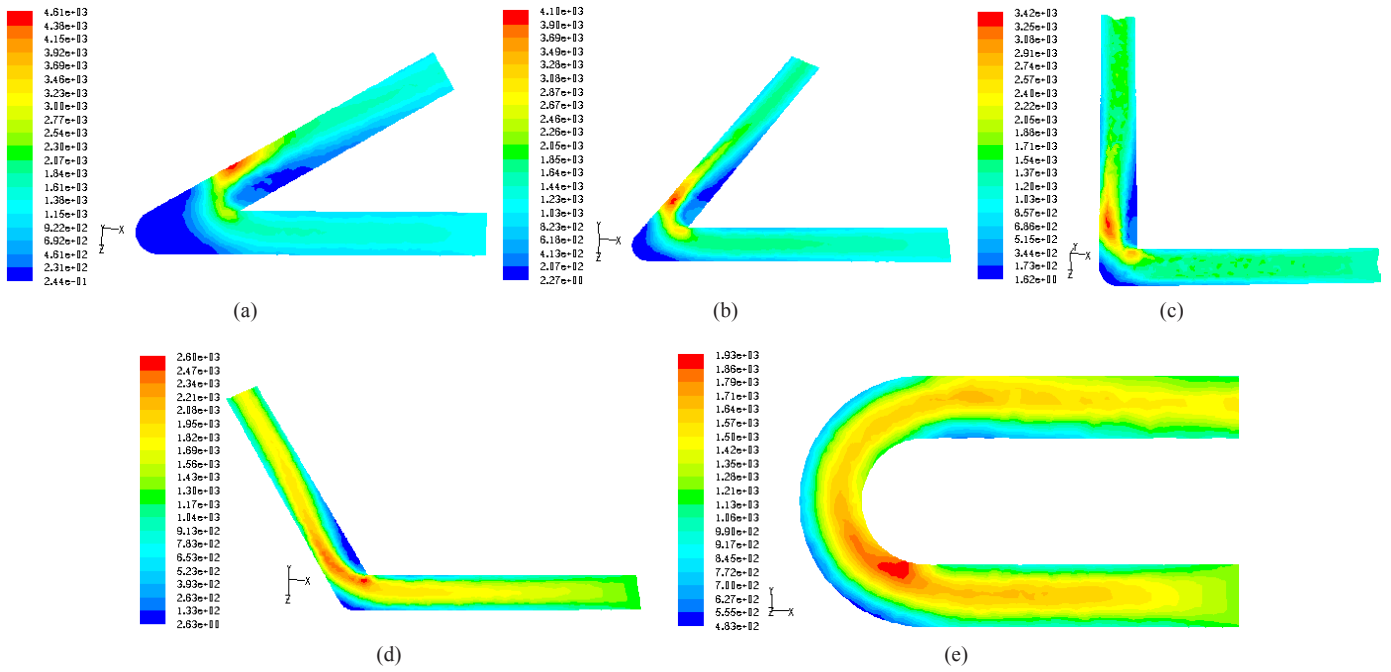


Fig. 10 Contours of dynamic pressure (Pa) of the bends (a) 30° (b) 60° (c) 90° (d) 120° (e) U-bend, SMC solution Conc. (kg/m³): 0.8, Q_i(m³/s): 20 x 10⁻⁵

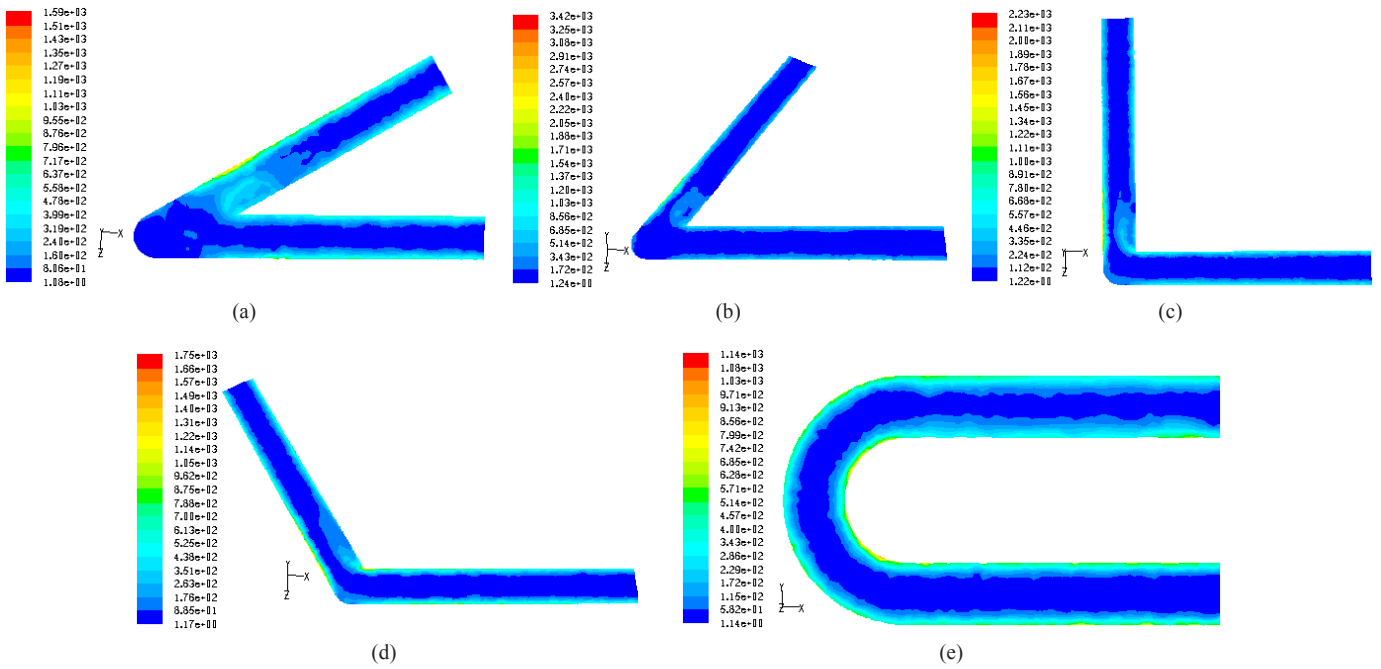


Fig. 11 Contours of vorticity magnitude (1/s) of the bends (a) 30° (b) 60° (c) 90° (d) 120° (e) U-bend, SMC solution Conc. (kg/m³): 0.8, Q_i(m³/s): 20 x 10⁻⁵

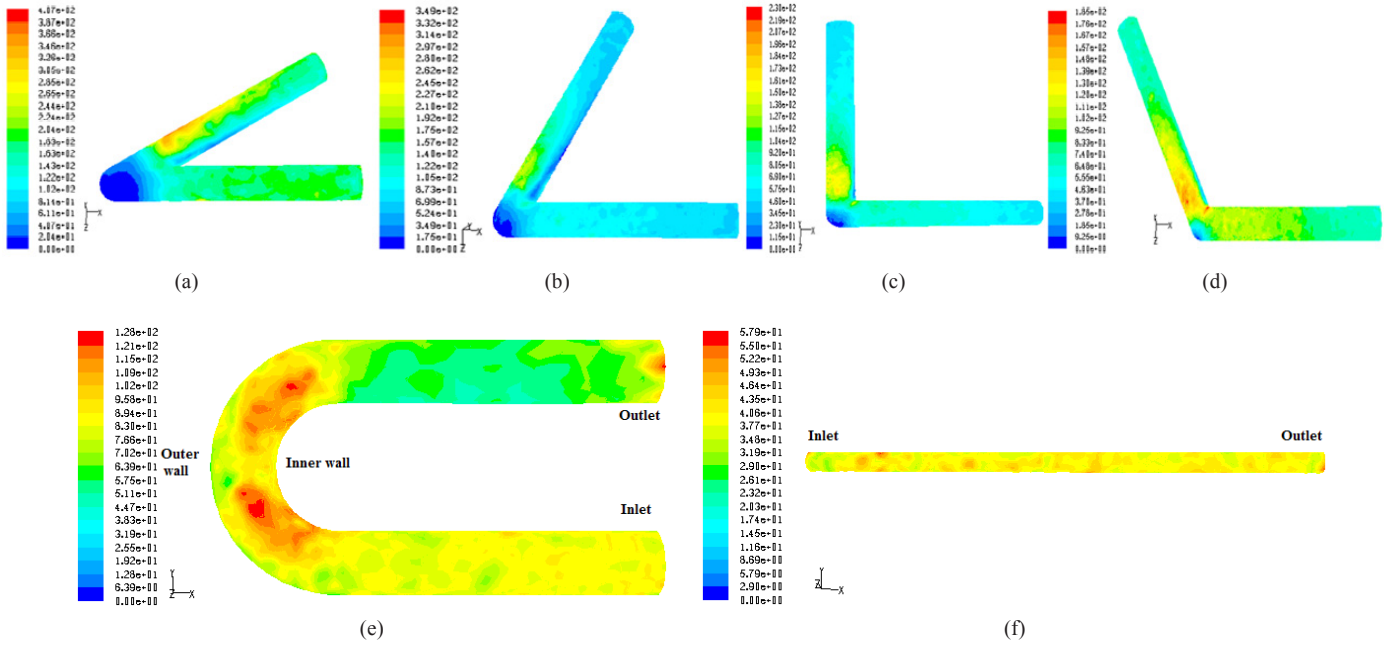


Fig. 12 Contour plot of shear stress (Pa) of the bends (a) 30° (b) 60° (c) 90° (d) 120° (e) U-bend (f) straight pipe, SMC solution Conc. (kg/m³): 0.8, Q_v(m³/s): 45 x 10⁻⁵

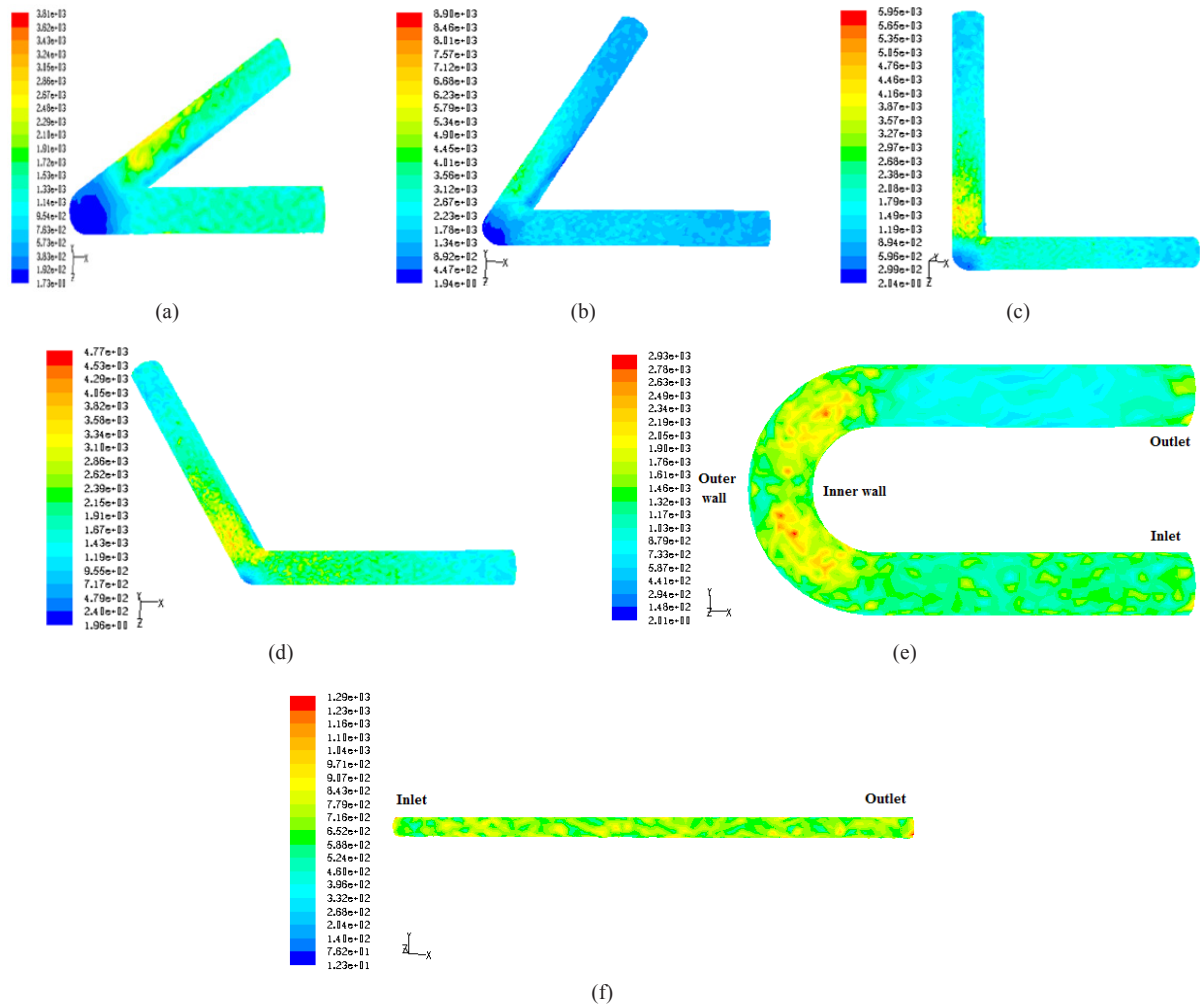


Fig. 13 Contour plot of shear strain rate (1/s) of the bends (a) 30° (b) 60° (c) 90° (d) 120° (e) U-bend (f) straight pipe, SMC solution Conc. (kg/m³): 0.8, Q_v(m³/s): 45 x 10⁻⁵

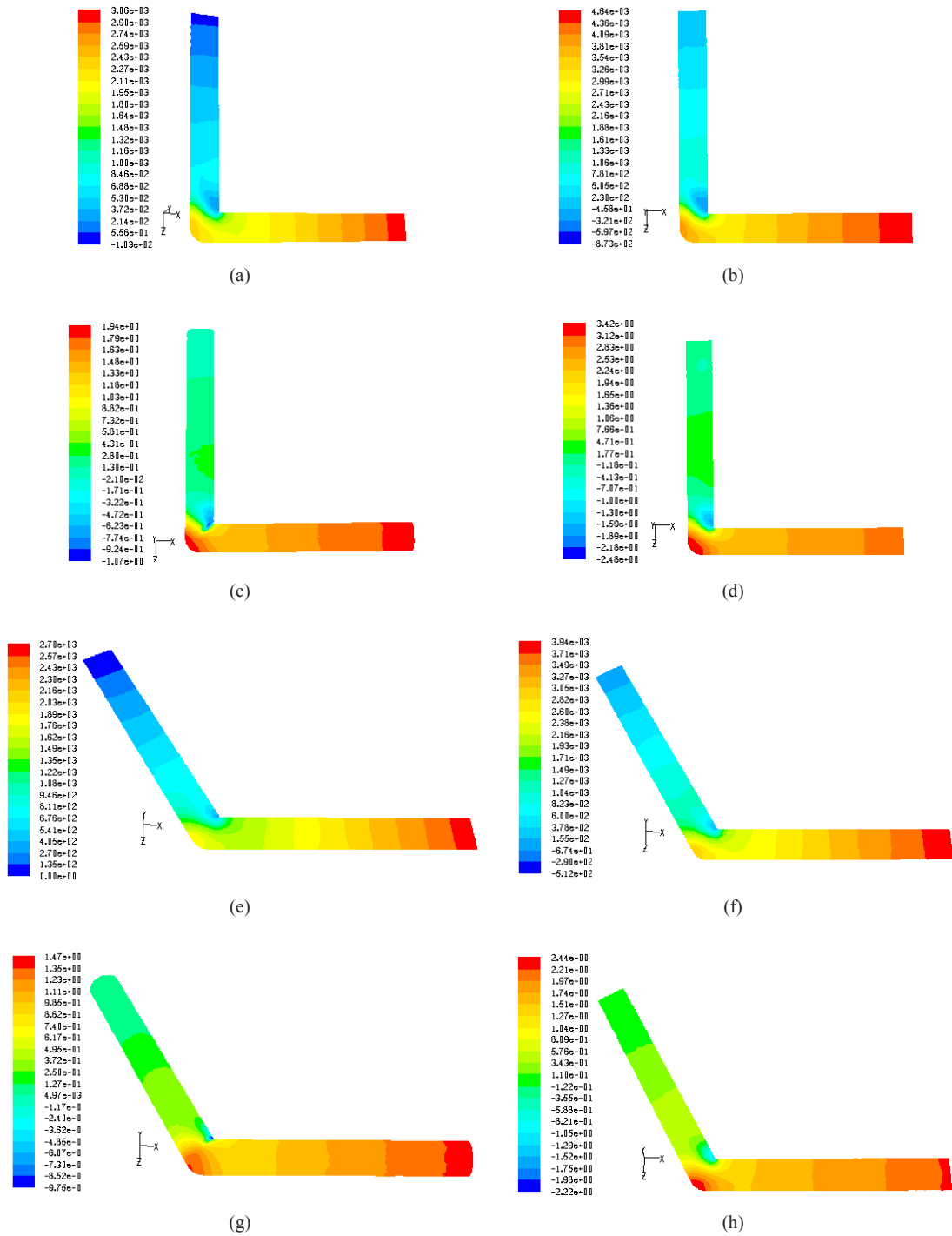


Fig. 14 Contour plot of static pressure (Pa) (a) - (b) for 90° bends and (e) - (f) for 120° bends for SMC solution Conc. (kg/m³): 0.8 and (c) - (d) for 90° bends and (g) - (h) for 120° bends for water at low and high flow rate Q_l(m³/s): 14.12 x 10⁻⁵ and 20 x 10⁻⁵

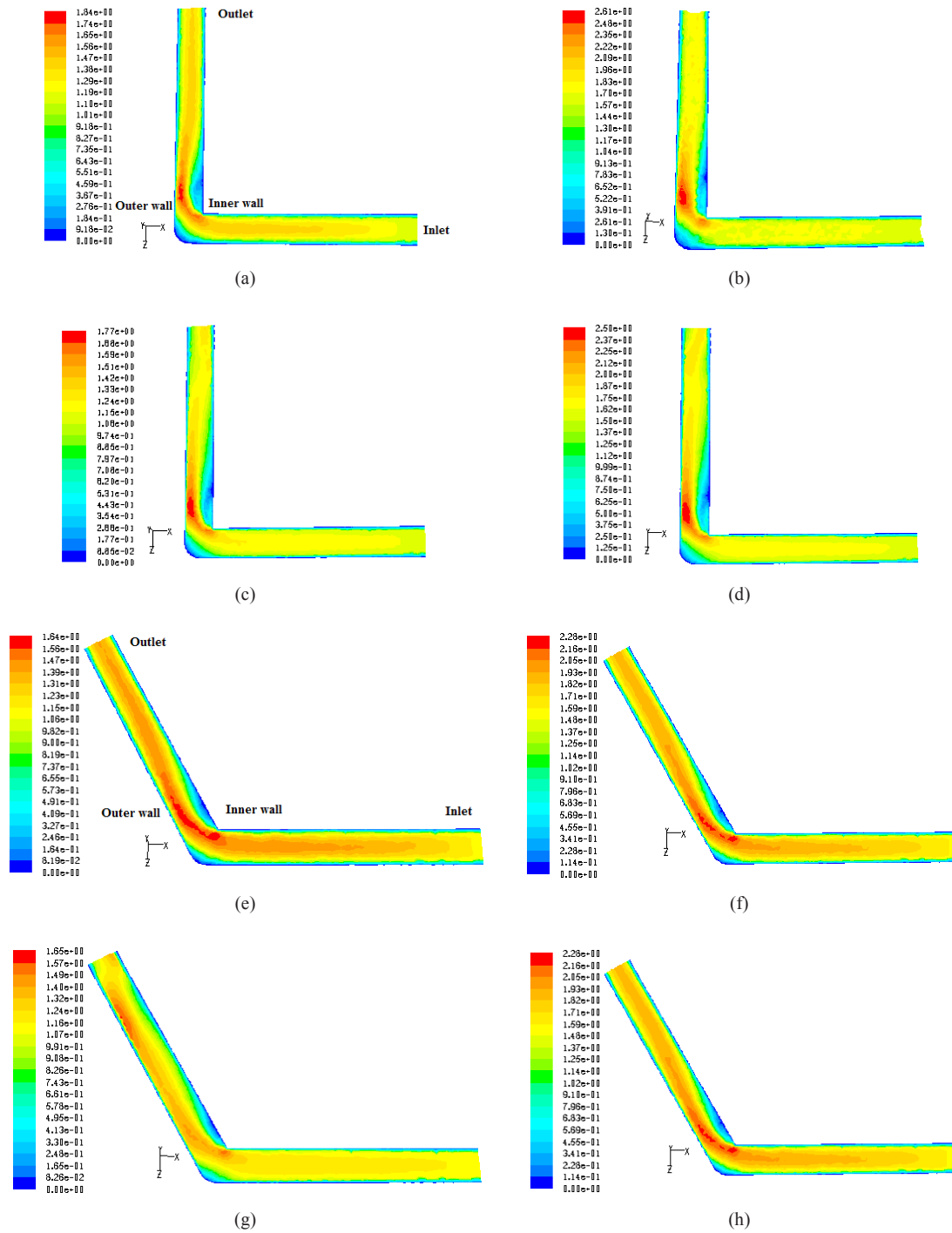


Fig. 15 Contour plot of velocity magnitude (m/s)(a)- (b) for 90° bends and (e) -(f) for 120° bends for SCMC solution Conc. (kg/m³): 0.8 and (c) - (d) for 90° bends and (g) -(h) for 120° bends for water at low and high flow rate Q (m³/s): 14.12×10^{-5} and 20×10^{-5}

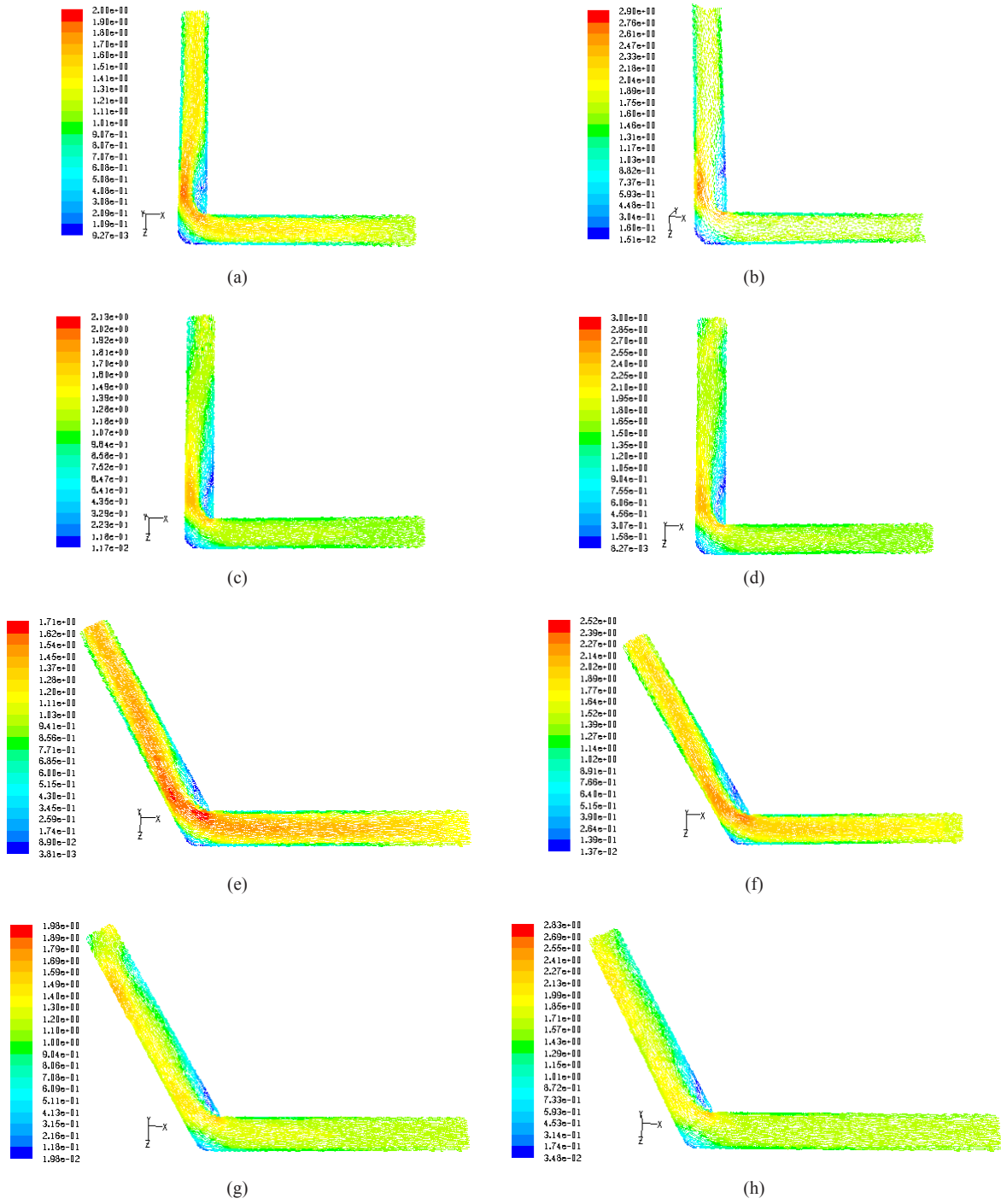


Fig. 16 Contour plot of velocity vector (m/s) (a) - (b) for 90° bends and (e) - (f) for 120° bends for SCMC solution Conc. (kg/m³): 0.8 and (c) - (d) for 90° bends and (g) - (h) for 120° bends for water at low and high flow rate Q_i(m³/s): 14.12 x 10⁻⁵ and 20 x 10⁻⁵

5.7 Effect of Non-Newtonian Characteristics on single-phase pressure drop, velocity, and shear stress and strain

Fig. 17, Fig. 18, Fig. 19, Fig. 20 show the effect of non-Newtonian liquid characteristic of single-phase pressure drop for 90° bend and velocity, shear stress and strain of the 120° bend. It is clear from the plot that as n' decreases the single-phase pressure drop, velocity, shear stress and strain increases

at a constant liquid flow rate. The effective viscosity increases as n' decreases and hence the single-phase pressure drop, velocity, shear stress and strain across the bend increases at a constant liquid flow rate. It was also seen that the shear stress and strain are more near the wall side compared to the central position of the pipe bend as velocity variation between the fluid layers is more near the wall side compared to the central position.

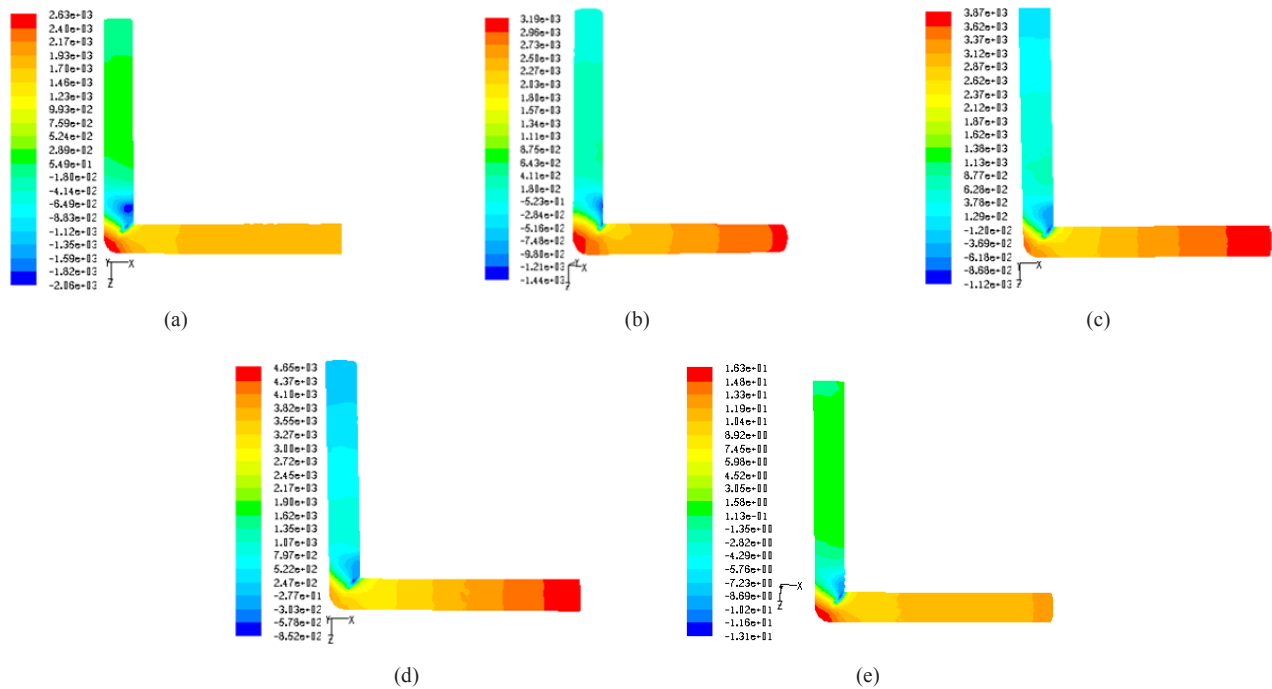


Fig. 17 Contour plot of static pressure (Pa) inside the different points of the 90° bends for SMC solution flow rate, Q_1 (m³/s): 20×10^{-5} and Conc. (kg/m³): (a) 0.2 (b) 0.4 (c) 0.6 (d) 0.8 (e) water.

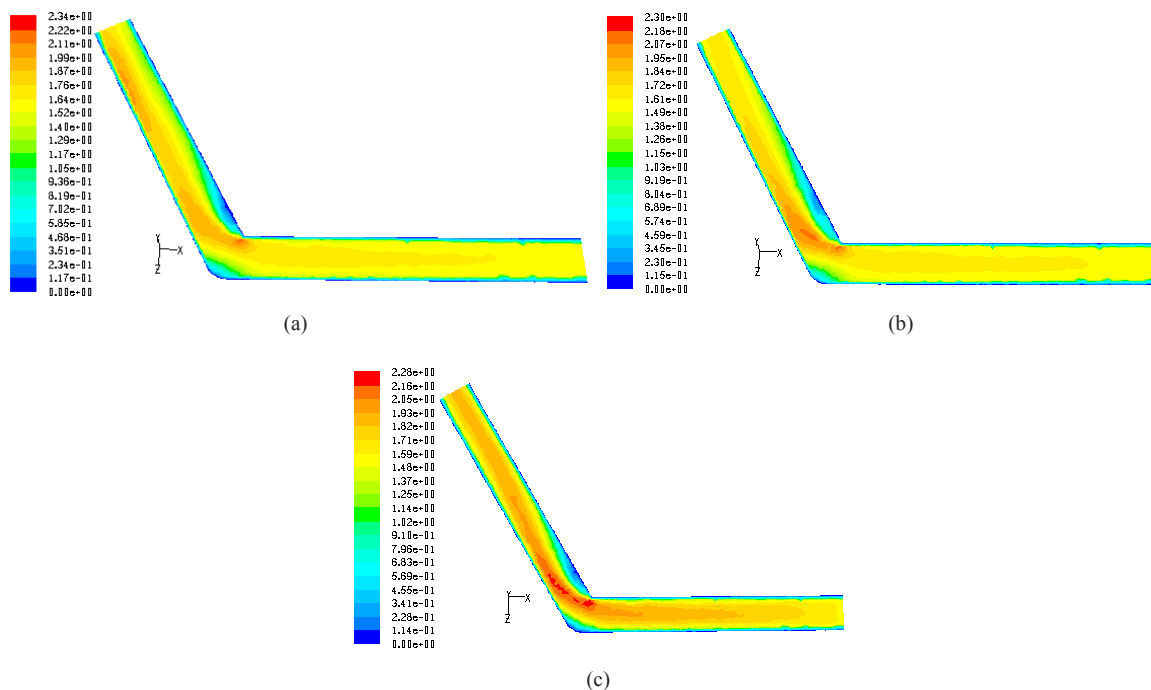


Fig. 18 Contour plot of velocity magnitude (m/s) of the 120° bends for SMC solution flow rate, Q_1 (m³/s): 20×10^{-5} and Conc. (kg/m³): (a) water (b) 0.2 and (c) 0.8

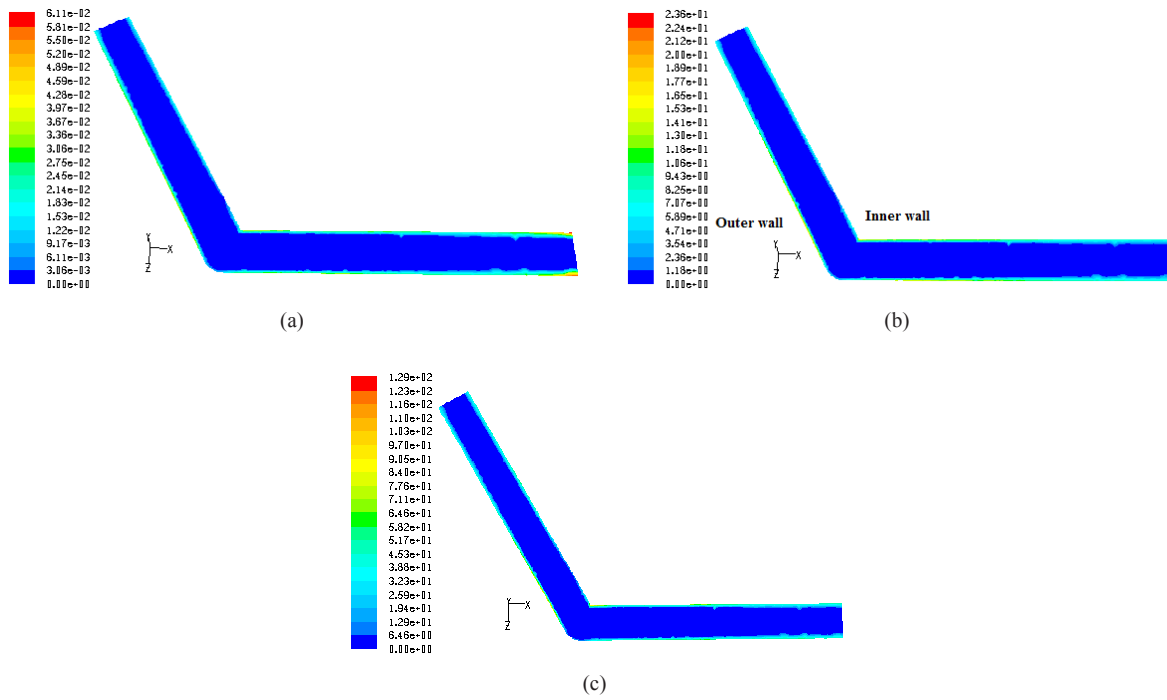


Fig. 19 Contour plot of wall shear stress (Pa) of the 120° bends for SCMC solution flow rate, $Q(\text{m}^3/\text{s}): 20 \times 10^{-5}$ and Conc. (kg/m^3): (a) water (b) 0.2 and (c) 0.8

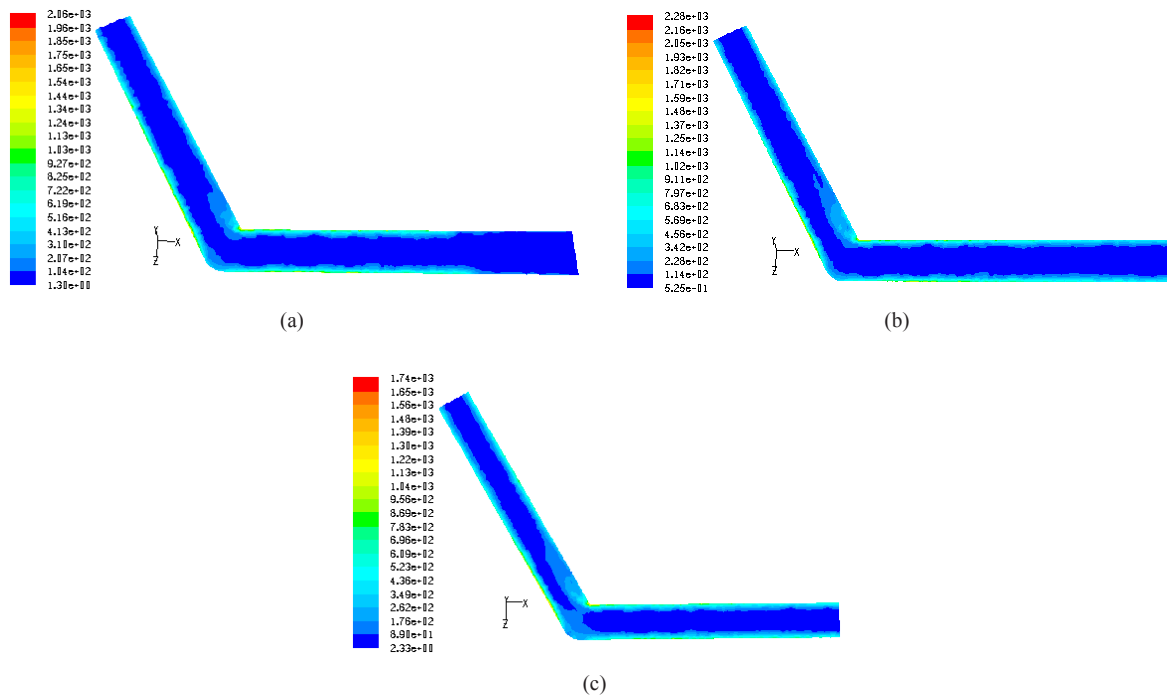
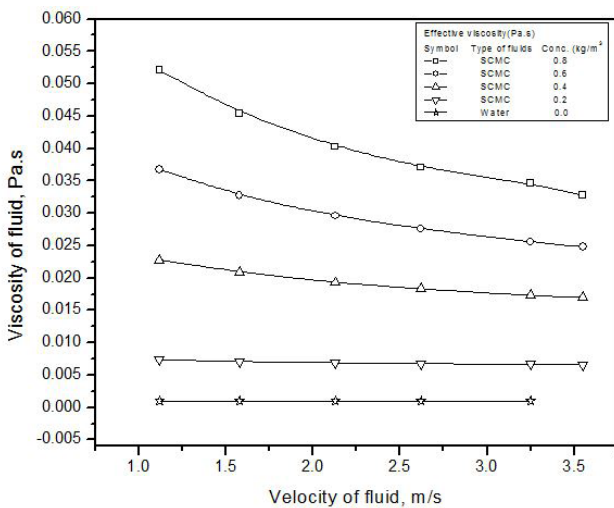


Fig. 20 Contour plot of wall strain rate (1/s) of the 120° bends for SCMC solution flow rate, $Q(\text{m}^3/\text{s}): 20 \times 10^{-5}$ and Conc. (kg/m^3): (a) water (b) 0.2 and (c) 0.8

5.8 Validation plot

Fig. 21 (a) shows that the effective viscosity decreases with increasing velocity of fluids for SCMC solution, but for water it is unchanged. This is due to the non-Newtonian pseudo plastic behavior of SCMC solution and Newtonian fluid behavior of water. Fig. 21(b) shows that static pressure distribution in the upstream, downstream and bend portion for a fixed solution flow rate. The static pressure increases with increase in the SCMC solution flow rate. The CFD simulated data is well matched with experimental results. Fig. 22 (a) indicates that the variation of pressure drop across the bends with liquid flow rate for different bend angles and Fig. 22 (b) indicates that the variation of pressure drop across the bends with liquid flow rate for different SCMC solution. The pressure drop increases with decrease in bend angle and increases with SCMC solution concentration. For both the cases, CFD simulated results are validated with experimental results. Fig. 23 (a) illustrates the velocity profile of Newtonian and non-Newtonian fluids across radial position in a straight circular pipe. The profiles for pseudo plastic fluids (SCMC) are flatter and true parabolic for water (Newtonian). Fig. 23 (b) illustrates the velocity profile of Newtonian and non-Newtonian fluids across radial position in bends. The profile for pseudo plastic fluids (SCMC) are flatter and steep for water (Newtonian). When fluid enters into the bend portion, it moves to the outer wall side due to centrifugal force and again after collision with wall, fluid returns to the inner wall side and hence velocity is distributed in the bend. The SCMC solution shifted more to the wall side compared to water as generation of intensified centrifugal force from more angular momentum is compared to less dense water. In both cases, experimental results are validated with CFD results.



(a)

5.8.1 Loss coefficient

The reduction in static head for flow through a pipe bend in a pipe line can be expressed in terms of velocity head and the resistance coefficient or loss coefficient, k_l . The bend is characterized by k_l and the frictional energy loss, h_{fb} is evaluated as,

$$h_{fb} = \frac{\Delta P_b}{\rho_l} = \frac{k_l u_l^2}{2} \tag{14}$$

Fig. 24 (a) shows the comparison plot of loss coefficients for different bends. From this plot, we observe that the loss coefficient decreases with increasing bend angle.

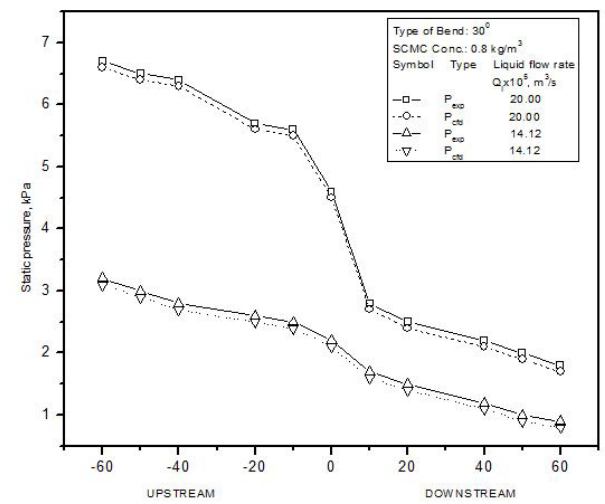
Fig. 24 (b) illustrates the variation of friction factor with Dean Number for non-Newtonian pseudo plastic fluid flow through different bends. From this plot we observe that friction factor decreases with Dean Number and it was remarkably more for 30° bend compared to the other bends.

5.8.2 Analysis of the experimental pressure drop

The pressure drop were first measured in a straight horizontal tube to test or verify the accuracy of the experimental techniques and procedure. The results were found to be in close agreement with the conventional resistance formula used for non-Newtonian pseudo plastic liquid flow through straight pipe in laminar flow condition. The formula is expressed as,

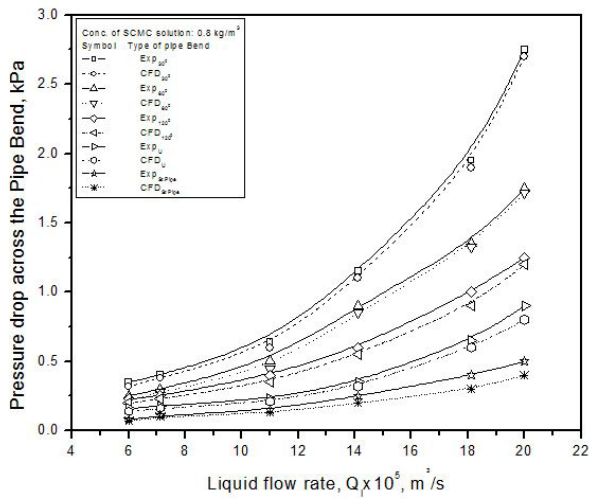
$$f_s = \frac{16}{Re} \tag{15}$$

The plot of friction factor vs. Reynolds number for the straight horizontal pipe in laminar flow condition has been shown in the Fig. 25 (a). The plot signifies the accuracy of the experimental procedure and techniques. The experimental results are tested by CFD analysis and well matched.

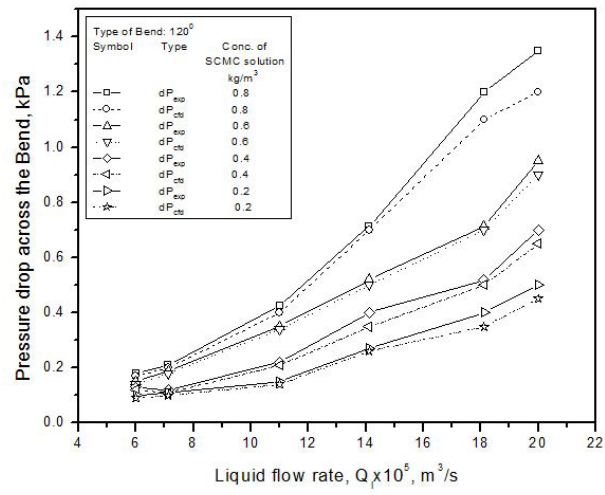


(b)

Fig. 21 (a) Variation of viscosity with fluid velocity for SCMC solution and water, (b) comparison plot of experimental and CFD for 30° bend

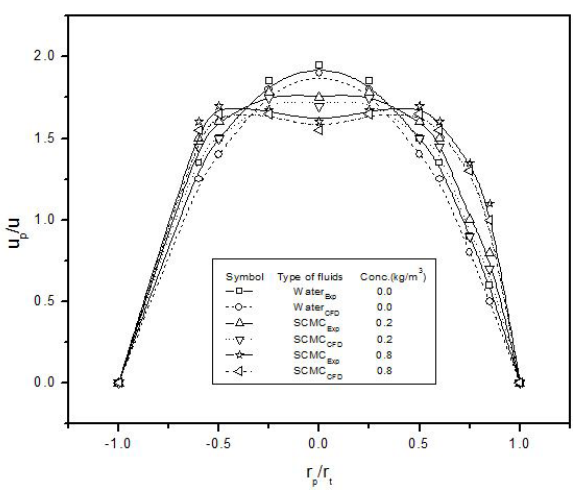


(a)

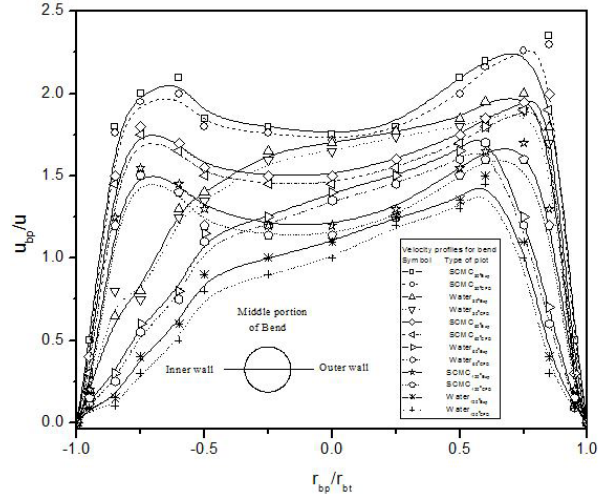


(b)

Fig. 22 (a) variation of pressure drop across the bends with liquid flow rate (b) comparison plot of pressure drop across the bends versus liquid flow rate at different SCMC solution concentration (kg/m^3): 0.2 - 0.8

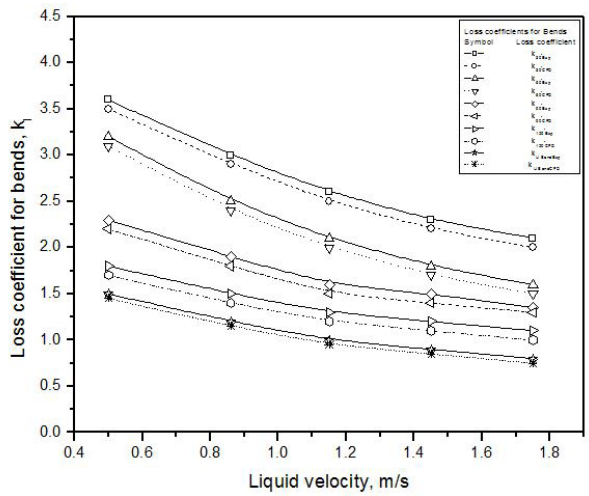


(a)

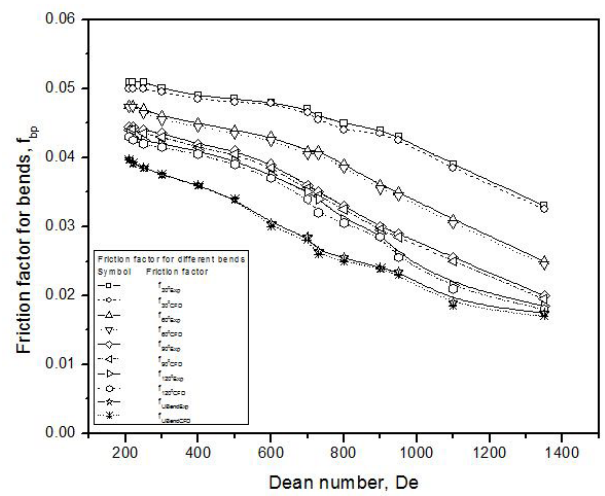


(b)

Fig. 23 Velocity profiles for water and SCMC solution flow through (a) straight pipe and (b) bends

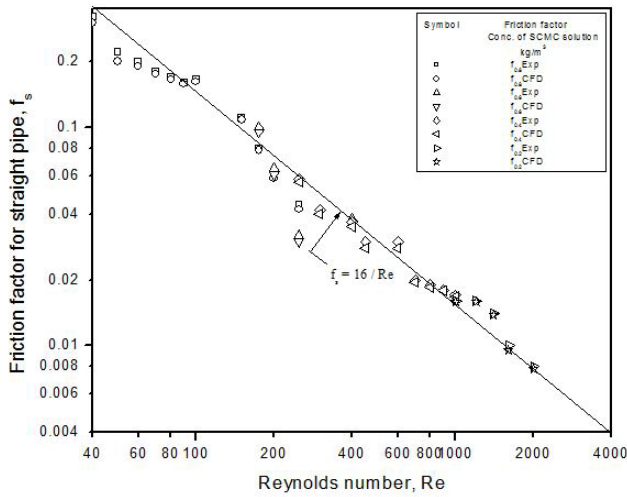


(a)

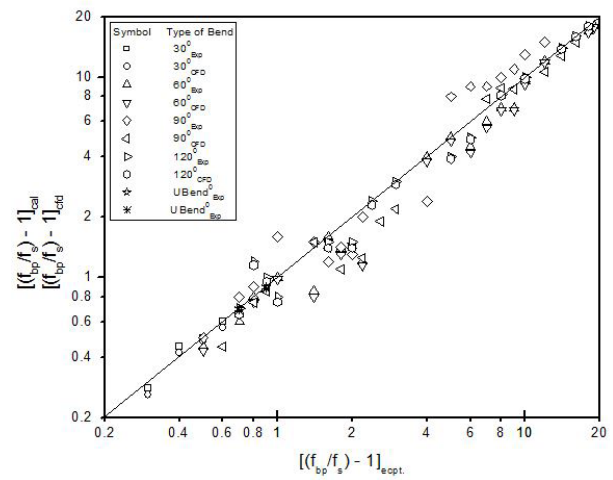


(b)

Fig. 24 Comparison plot of experimental and CFD simulated data for (a) loss coefficients of different types of bends with 0.8 kg/m^3 SCMC solution (b) friction factor vs. Dean Number



(a)



(b)

Fig. 25 (a) Plot of f_s vs. Re for straight pipe (b) Plot of $[(f_{bp}/f_s) - 1]_{cal}$ vs. $[(f_{bp}/f_s) - 1]_{expt}$ for all types of bends in horizontal plane.

The following functional relationship is developed from the Eq. (6) for bends with the help of multivariable linear regression analysis:

$$\left[\left(\frac{f_{bp}}{f_s} \right) - 1 \right] = (4.52 \times 10^{-2}) [De_{bp}]^{(0.756 \pm 0.062)} \times \left[\frac{\alpha}{180} \right]^{(-0.532 \pm 0.196)} \quad (16)$$

For, $40 < Re < 2100$, $30 < De < 2050$, $30 < \alpha < 120^\circ - 180^\circ$

The predicted values of $[(f_{bp}/f_s) - 1]$ from the above equation against the experimental values have been plotted in the Fig. 25 (b). The experimental results are tested by CFD analysis and well matched.

The correlation coefficient and variance of estimate are 0.92 and 0.1612 respectively for a 't' value of 1.96 and 134 degrees of freedom(t) at 0.06 probability level and 94% confidence range.

6 Conclusions

1. The frictional pressure drop for non-Newtonian liquid flow through bends is measured experimentally.
2. A CFD based software Fluent (Fluent user guide, USA [28] has been used for CFD analysis. The tetrahedral grid is used for simulation purpose and compared their suitability.
3. Pressure drop, friction factor, flow structure analysis across the different pipe bends have also been done.
4. The Pressure drop will be more in the case 300 bend compared to 1200 and U bend. CFD has clearly analyzed it.
5. The Comparison plot of the loss coefficients for the different types of bends is drawn. The loss coefficients are more for 300 bend and less for 1200 and U-bend. CFD validates the experimental data.
6. CFD predicts the effect of flow structure, liquid concentration, i.e., pseudo plasticity, friction factor, shear stress, shear strain and cell Reynolds no. on frictional pressure.
7. The following flow phenomena inside the bends are observed:

7.a The maximum velocity and maximum pressure is shifted towards the outer wall due to centrifugal force.

7.b Vortices are created at different location of the bend.

8. CFD analyzed the friction factor, pressure drop for SCMC and water flow through straight and bend pipe in the smaller Reynolds number region and also in a higher Reynolds number region.
9. CFD and experimental data were compared critically.
10. A generalized correlation has been developed. This is used to predict the frictional pressure drop across the different pipe bends in the horizontal plane for non-Newtonian pseudo plastic power law fluids in laminar flow condition. CFD validated the established correlation.
11. The non-Newtonian liquids used consisted of different concentrations of sodium salt of carboxy methyl cellulose which behaved like pseudo plastic fluids.

Nomenclature

K'	consistency index $[Ns^n / m^2]$;
d	diameter $[m]$;
De	Dean Number;
n'	flow behavior index;
f	friction factor;
h	frictional energy loss;
k	friction coefficient;
L	length $[m]$;
P	pressure $[N/m^2]$, $[Pa]$ or $[kPa]$;
r	radius $[m]$;
Re	Reynolds Number;
u	velocity $[m/s]$;

Greek symbols

α	angle $[degree]$;
ρ	density $[kg/m^3]$;

Δ	drop;
ν	kinematic viscosity [m^2/s];
τ	shear stress [N/m^2];
μ	viscosity [$\text{Pa}\cdot\text{s}$];

Subscripts

z	axial direction;
θ	angular direction;
bp	bend pipe;
b	bend;
cb	curvature of bend
xy	direction;
eff	effective;
l	liquid;
p	pipe;
r	radial direction;
s	straight;

References

- Dean, W. R. "Fluid motion in a curved channel." *Proceedings of the Royal Society of London. Series A, Containing Papers of a Mathematical and Physical Character*. 121(787), pp. 402-420. 1928. <https://doi.org/10.1098/rspa.1928.0205>
- Dean, W. R. "The Stream-line motion in curved pipes." *The London, Edinburgh, and Dublin Philosophical Magazine and Journal of Science*. 5(31), pp. 673-693. 1928. <https://doi.org/10.1080/14786440408564513>
- Berger, S. A., Talbot, A., Yao, L. S. "Flow in Curved Pipes." *Annual Review of Fluid Mechanics*. 15, pp. 461-512. 1983. <https://doi.org/10.1146/annurev.fl.15.010183.002333>
- Soh, W., Berger, S. A. "Laminar entrance flow in a curved pipe." *Journal of Fluid Mechanics*. 148, pp. 1984. <https://doi.org/10.1017/S0022112084002275>
- Das, S. K., Biswas, M. N., Mitra, A. K. "Friction factor for gas-non-newtonian liquid flow in horizontal bends." *The Canadian Journal of Chemical Engineering*. 69(1), pp. 179-187. 1991. <https://doi.org/10.1002/cjce.5450690121>
- Mashelkar, R. A., Devarajan, G. V. "Secondary flows of non-Newtonian fluids: Part I – laminar boundary layer flow of a generalized non-Newtonian fluid in a coiled tube." *Transactions of the Institution of Chemical Engineers*. 54, pp. 100-107. 1976.
- Mishra, P., Gupta, N. "Momentum transfer in curved pipes. 2. Non-Newtonian fluids." *Industrial & Engineering Chemistry Process Design and Development*. 18(1), pp. 137-142. 1979.
- Edwards, M. F., Jadallah, M. S. M., Smith, R. "Head losses in pipe fittings at low Reynolds numbers." *Chemical Engineering Research and Design*. 63, pp. 43-50. 1985.
- Bandyopadhyay, T. K., Das, S. K. "Non-Newtonian pseudo plastic liquid flow through small diameter piping components." *Journal of Petroleum Science and Engineering*. 55(1-2), pp. 156-166. 2007. <https://doi.org/10.1016/j.petrol.2006.04.006>
- Bandyopadhyay, T. K., Das, S. K. "Non-Newtonian and Gas-non-Newtonian Liquid Flow through Elbows – CFD Analysis." *Journal of Applied Fluid Mechanics*. 6(1), pp. 131-141. 2013. URL: http://www.sid.ir/en/VEWSSID/J_pdf/112520130115.pdf
- Hidayat, M., Rasmuson, A. "Numerical investigation of gas-solid flow in a U-bend." In: *Proceedings of the 13th International Drying Symposium*, Beijing, China, pp. 424-433. 2002.
- Marn, J., Ternik, P. "Laminar flow of a shear-thickening fluid in a 90° pipe bend." *Fluid Dynamics Research*. 38(5), pp. 295-312. 2006. <https://doi.org/10.1016/j.fluiddyn.2006.01.003>
- Kuan, B., Yang, W., Solnordal, C. "CFD simulation and experimental validation of dilute particulate turbulent flows in a 90° duct bend." In: *Third International Conference on CFD in the Minerals and Process Industries*. CSIRO, Melbourne, Australia, Dec. 10-12, 2003. pp. 531-536. URL: http://www.cfd.com.au/cfd_conf03/papers/084Kua.pdf
- Shah, S. N., Jain, S. "Coiled tubing erosion during hydraulic fracturing slurry flow." *Wear*. 264(3-4), pp. 279-290. 2008. <https://doi.org/10.1016/j.wear.2007.03.016>
- Wu, B., Chen, S. "CFD simulation of non-Newtonian fluid flow in anaerobic digesters." *Biotechnology and Bioengineering*. 99(3), pp. 700-711. <https://doi.org/10.1002/bit.21613>
- Manzar, M. A., Shah, S. N. "Particle distribution and erosion during the flow of Newtonian and non-newtonian slurries in straight and coiled pipes." *Engineering Applications of Computational Fluid Mechanics*. 3(3), pp. 296-320. 2008. <https://doi.org/10.1080/19942060.2009.11015273>
- Kalpikli, A. "Experimental study of turbulent flows through pipe bends." Technical Reports from Royal Institute of Technology, KTH Mechanics, Stockholm, Sweden. 2012. URL: http://www.mech.kth.se/thesis/2012/lic/lic_2012_athanasia_kalpikli.pdf
- Rani, H. P., Sheu, T. W. H., Chang, T. M., Liang, P. C. "Numerical investigation of non-Newtonian microcirculatory blood flow in hepatic lobule." *Journal of Biomechanics*. 39(3), pp. 551-563. 2006. <https://doi.org/10.1016/j.jbiomech.2004.11.029>
- Doorly, D., Sherwin, S. "Geometry and flow." In: *Cardiovascular Mathematics. Modeling and simulation of the circulatory system*. (Formaggia, L., Quarteroni, A., Veneziani, A. (eds.)), Springer Verlag, Italia, Milano, 2009.
- Kadyirov, A. "Numerical investigation of swirl flow in Curved Tube with various Curvature Ratio." In: *Excerpt from the Proceedings of the 2013 COMSOL Conference in Rotterdam*. 2013. URL: https://www.comsol.com/paper/download/181987/kadyirov_paper.pdf
- Mikhail, T. A., Aissa, W. A., Hassanein, S. A., Handy, O. "CFD simulation of dilute gas-solid flow in 90° squares bend." *Energy and Power Engineering*. 3(3), pp. 246-252. 2011. <https://doi.org/10.4236/epe.2011.33031>
- Spedding, P. L., Benard, E. "Gas-liquid two-phase flow through a vertical 90° elbow bend." *Experimental Thermal and Fluid Science*. 37(1), pp. 761-769. 2007. <https://doi.org/10.1016/j.expthermflusci.2006.08.003>
- Ito, H. "Flow in curved pipes." *JSME International Journal*. 30(262), pp. 543-552. 2008. <https://doi.org/10.1299/jsme1987.30.543>
- Jayanti, S., Wang M. J. "Gas particle flow through bends." *IMeChE*, C461/024, 161-166. URL: https://www.td.mw.tum.de/fileadmin/w00b-so/www/Forschung/Publikationen_Mayingner/222.pdf
- Berger, S. A., Jou, L.-D. "Flows in stenotic vessels." *Annual Review of Fluid Mechanics*. 32, pp. 347-382. 2000. <https://doi.org/10.1146/annurev.fluid.32.1.347>
- Gijzen, F. J. H., van de Vosse, F. N., Janssen, J. D. "The influence of the non-Newtonian properties of blood on the flow in large arteries: unsteady flow in a 90° curved tube." *Journal of Biomechanics*. 32(7), pp. 705-713. 1999. [https://doi.org/10.1016/S0021-9290\(99\)00014-7](https://doi.org/10.1016/S0021-9290(99)00014-7)
- Tanaka, M., Wada, S., Nakamura, M. "Mechanics of Biofluids and Computational Analysis." In: *Computational Biomechanics*. pp. 87-140. Springer Japan, 2012. https://doi.org/10.1007/978-4-431-54073-1_3
- Fluent Users Guide, Version 6.3, Fluent India, Pune, 2008.